UNIVERSITY OF NAPLES FEDERICO II

DOCTORATE
MOLECULAR MEDICINE AND MEDICAL BIOTECHNOLOGY

XXX CYCLE

AFFINITY MATURATION OF NOVEL HUMAN ANTIBODIES FOR CANCER IMMUNOTHERAPY, BY YEAST SURFACE DISPLAY TECHNOLOGY

Tutor
Prof. Alfredo Nicosia

Candidate
Biancamaria Cembrola

COORDINATOR

Prof. Vittorio Enrico
Avvedimento

Academic Year 2016/2017

INDEX

ABSTRACT **1**

ABBREVIATIONS **2**

1. INTRODUCTION **4**

1.1. Antibodies as therapeutics 4

1.2. In vivo antibody affinity maturation 4

1.3. In vitro antibody affinity maturation 7

1.4. Affinity maturation by yeast surface display (YSD) 8

1.5. Antibodies with potential therapeutic application, isolated by YSD 13

1.6. Antibodies in cancer treatment 14

1.7. Role of the immune surveillance in cancer progression and development of immune escape mechanisms 15

1.8. The immune checkpoints - the PD-1/PD-L1 pathway and its role in the regulation of T cell functioning 16

1.9. Impairment of PD-1/PD-L1 pathway in cancer 20

1.10. Targeting of immune checkpoints with mAbs 23

2. AIM **26**

3. MATERIALS AND METHODS **27**

3.1. Cell lines and culture media 27

3.2. Bacterial strains and culture media 27

3.3. Yeast strains 27

3.4. Yeast culture media 28

3.5. Plasmids 30

3.6. Bacterial transformation 30

3.7. Preparation of yeast competent cells 31

3.8. Yeast transformation 31

3.8.1. Generation of scFv-displaying yeast libraries 31

3.8.2. Generation of individual scFv-displaying yeast clones 32

3.9. Determination of the transformation efficiency.....32

3.10. Isolation of plasmid DNA from bacterial and yeast cultures 32

3.11. Determination of scFv CDRs.....33

3.12. Generation of repertoires of randomly mutated CDR3s.....33

3.13. Topo cloning 34

3.14. High-throughput sequencing analysis of the repertoires of mutated CDR3s.....34

3.15. Generation of full length mutated scFvs.....34

3.16. Flow cytometry binding assays.....36

3.17. Cell sorting.....37

3.18. Estimation of diversity of sorted yeast populations 37

3.19. mAb production.....38

3.20. mAb purification 38

3.21. Protein quantification and coomassie staining.....38

3.22. Flow cytometry binding assays of mAbs to hPBMCs 39

4. RESULTS 41

4.1. Multi-step and CDR-targeted random mutagenesis of an anti PD-L1 scFv.....41

4.2. High-throughput sequencing of the different repertoires of mutants.....43

4.3. Generation of CDR3-mutated D25 yeast libraries.....46

4.4. Set up of flow cytometry analyses for library selection.....48

4.5. Cell sorting-based selection of high affinity anti-PD-L1 scFvs from the library 3 51

4.6. Cell sorting-based selection of high affinity anti-PD-L1 scFvs from library 10 53

4.7. Flow cytometry analysis of PD-L1 binding to the sorted populations from library 3 and library 10 54

4.8. Sequencing of random clones from the yeast populations selected from library 3 and 10.....56

4.9. Generation of the individual mutated yeast clones and binding assay to PD-L1 58

4.10. Characterization of the individual yeast-scFv clones.....61

4.11. Generation, expression and purification of D25 full-length IgGs.....64

4.12. Binding assays of the mutated IgGs to hPBMCs 65

5. DISCUSSION 69

6. CONCLUSIONS 75

7. REFERENCES.....77

ABSTRACT

The affinity engineering is a key step to increase the therapeutic efficacy of monoclonal antibodies (mAbs). Yeast surface display (YSD) is the most widely used and powerful affinity maturation approach, allowing for the achievement of low picomolar antibody binding affinities. A great number of mAbs approved for clinics are used in cancer immunotherapy, for the targeting of either tumor neoantigens or immune checkpoint components; this second approach aims to re-activate the T cell-mediated anti-tumor immunity, which is often impaired by cancer cells through several immune escape mechanisms.

In this study, we describe an optimization of the YSD methodology, applied to the generation of potentially therapeutic high affinity single chain antibody fragments (scFv) targeting PD-L1, an immune checkpoint component which is often upregulated on cancer cell surface. To generate yeast libraries with high mutant frequency and diversity, we performed ten sequential error-prone PCR cycles involving the heavy chain variable region CDR3 of an anti PD-L1 scFv. We analyzed the ten CDR3 pools by high-throughput sequencing and, basing on the frequencies of wild type and mutated sequences observed in each pool, as well as the stop codon frequency and the number of mutation per sequence, we chose pools obtained from mutagenesis rounds 3 and 10 to generate two different mutant scFv-yeast libraries with high theoretical complexities (2×10^8 and $1{,}7 \times 10^8$, respectively). By fluorescence-activated cell sorting (FACS) we quickly isolated yeast subpopulations with improved antigen binding capacity for soluble PD-L1, using a high-low antigen concentration selection scheme that reduced the chance to sort the wild type clones present in the library.

By Sanger sequencing of just 24 randomly chosen yeast clones from each of the two sorted libraries, we identified 6 enriched scFv-yeast clones, showing a 6,3- to 9,8-fold affinity improvement compared with the parental one. In addition, the mutated positions and the kind of amino acid substitutions were extremely conserved in the clones selected from the two different libraries, suggesting the presence of mutation hotspots that could be identified independently from the number of mutagenesis rounds performed. These scFvs maintained some binding improvement also when converted into IgGs and tested on PD-L1 protein showed on the plasma membrane of human activated lymphocytes. These antibodies, isolated through a faster and more effective YSD approach, could be very good candidates for an antibody-based, PD-L1-targeted cancer immunotherapy.

ABBREVIATIONS

ADCC: antibody-dependent cellular cytotoxicity
ADEPT: antibody-directed enzyme prodrug therapy.
AID: activation-induced cytidine deaminase
APCs: antigen presenting cells
BATF: basic leucine zipper transcriptional factor ATF-like
BCR: B cell receptor
BSA: albumine from bovine serum
BTLA: B- and T-lymphocyte attenuator
CDC: complement-dependent cytotoxicity
CDR: complementarity-determining region
CFU: colony forming units
CH1: first constant domain of heavy chain
CH2: second constant domain of heavy chain
CTLA-4: cytotoxic T lymphocyte–associated antigen 4
DC: dendritic cell
EBNA-1: Epstein Barr Nuclear Antigen 1
ep-PCR: error-prone Polymerase Chain Reaction
Fab: antigen-binding fragment
FACS: Fluorescence-activated cell sorting
FBS: Fetal Bovine Serum
Fc: crystallizable fragment
FDA: Food and Drug Administration
GITR: glucocorticoid-induced TNFR-related gene
GM-CSF: granulocyte-macrophage colony-stimulating factor
GPI: glycosylphosphatidylinositol
hPBMCs: human peripheral blood mononuclear cells
ICEB: Ice Cold Electroporation Buffer
ICOS: inducible costimulator
IFN-α: interferon-α
IFN-γ: interferon-γ
Ig: immunoglobulin
IL-10: interleukin-10
IL-15: interleukin-15
IL-2: interleukin-2
IL-21: interleukin-21
IL-4: interleukin-4
IL-6: interleukin-6
IL-7: interleukin-7
ITIM: immunoreceptor tyrosine-based inhibitory motif
ITSM: immunoreceptor tyrosine-based switch motif

Kd: equilibrium dissociation constant
k_{off}: dissociation rate
k_{on}: association rate
LAD: lithium acetate - dithiothreitol
LAG-3: lymphocyte-activation gene 3
LB: Luria-Bertani
Lck: lymphocyte-specific protein tyrosine kinase
LMP-2: low-molecular-weight protein 2
LMP-7: low-molecular-weight protein 7
mAbs: monoclonal antibodies
MDSC: myeloid-derived suppressor cell
MHC I: major histocompatibility complex-class I
NF-kB: nuclear factor-Kb
NK: natural killer cells
NSCLC: non-small cell lung cancer
OD: optical density
PBS: phosphate buffered saline
PD-1: programmed death-1
PD-L1: programmed death ligand-1
PD-L2: programmed death ligand-2
RCC: renal cell carcinoma
scFv: single chain variable fragment
SCLC: small cell lung cancer
SDS-PAGE: sodium dodecyl sulfate polyacrylamide gel electrophoresis
SH-2: Src homology 2
SHM: somatic hypermutation
SHP-2: Src homology phosphatase 2
STAT-3: signal transducer and activator of transcription 3
TAP: transporter associated with antigen presentation
TCR: T cell receptor
TGF-β: transforming growth factor-β
TIM-3: T cell immunoglobulin 3
TNFR: tumor necrosis factor receptor
TNF-α: tumor necrosis factor-α
VEGF: vascular endothelial growth factor
VH: heavy chain variable region
VL: light chain variable region
YNB: Yeast Nitrogen Base
YPD: Yeast-Peptone-Dextrose
YSD: yeast surface display
ZAP-70: zeta-chain-associated protein kinase 70

1. INTRODUCTION

1.1. Antibodies as therapeutics

Monoclonal antibodies (mAbs) are widely used as therapeutics in various kinds of medical applications, such as autoimmune diseases (Chan et al, 2010), infectious diseases (Casadevall et al, 2004; Hey, 2015), post-transplantation immunosuppressive regimens (Mahmud et al, 2010) and cancer (Carter, 2001).
Since 1986, 74 mAbs have been approved by Food and Drug Administration (FDA) (https://www.accessdata.fda.gov/scripts/cder/daf/) and hundreds are in clinical trials with 50 of them undergoing late-stage clinical studies (Reichert, 2017).
Although most of the therapeutic mAbs are whole antibodies (murine, chimeric, humanized or fully human), alternative antibody formats consisting in antibody fragments or single antibody domains are emerging; thanks to their smaller size, these non-canonical antibodies overcome some pharmacokinetic issues such as tissue penetration. This class of molecules includes single chain variable fragments (scFv), formed by an heavy and a light chain variable domain (VH and VL respectively), covalently linked to each other; derivatives of scFvs (diabodies, tribodies, tetrabodies); antigen-binding fragments, (Fab, mono- or bi-specific); minibodies, i.e. immunoglobulins lacking the first and second constant domains of heavy chains (CH1 and CH2) or even single VH domains (Holliger et al, 2005).
Whatever the antibody format, all these molecules can be engineered to reach the desired pharmacological effect by improving various properties, such as affinity, solubility and stability in buffer formulations suitable for injection in humans, pharmacokinetic properties, immunogenicity and effector functions (if the molecule retains any effector domain). To improve the binding characteristics of an antibody, the variable region is usually engineered and it is not unusual that manipulating this region has an impact on all the other above properties too; on the contrary, changes in the constant region or crystallizable fragment (Fc) usually affect only the antibody effector functions (Igawa et al, 2011).

1.2. In vivo antibody affinity maturation

The binding of an antibody to its antigen is a reversible process in which the speed of association/dissociation depends on two kinds of forces. The first one is called affinity and it measures the binding strength of a single antibody to its ligand partner; the affinity is measured through the equilibrium

dissociation constant (Kd) that is a ratio of the antibody dissociation rate (k_{off}) to the antibody association rate (k_{on}) and it is inversely correlated with affinity. The other force is called avidity and plays a key role in the formation of great immunocomplexes in which many antibodies bind simultaneously to many antigen molecules; for this reason, avidity measures the overall binding strength resulting from the contribution of each antibody binding site (Rudnick et al, 2009; Oda et al, 2004).

Antibodies developed for clinics should have very high affinities for their targets, ensuring a more effective therapy (for example the ability of the antibody to recognize very low concentrations of its target) and allowing for a reduction in the dosage or in the number and frequency of administrations, mainly thanks to longer dissociation rates. Thus, a newly discovered antibody (called "lead antibody") is frequently engineered to improve its affinity through a process called affinity maturation. The principles underlying this process are the same as those used *in vivo* by B cells during the immune response (Chowdhury et al, 1999).

Each naïve B lymphocyte, resident in lymph node follicles, expresses a different B cell receptor (BCR) also called immunoglobulin (Ig), able to recognize a specific and unique foreign antigen. The diversification of the B cell receptor *repertoire* is achieved during B cell differentiation through somatic recombination of three different kinds of genic segments, called V, D and J respectively, each present in many different copies in the human genome. Once rearranged in a specific combination, these fragments form the complete and unique sequence of the variable region of an antibody, enabling it to specifically recognize a single antigen (Roth, 2014). All these Igs share the same Fc region (M isotype) and, upon antigen stimulation, they are produced in a soluble format in order to neutralize the foreign antigen circulating in the blood. At the beginning of the B cell response, IgMs show a very weak binding strength for their own antigens (their affinities range between 10^-4 and 10^-6 mol/L), but when secreted, they are grouped into pentameric complexes having a high avidity for the antigen that is sufficient to ensure a first-line and effective protection. In the meantime, the B cell receptor locus undergoes various somatic rearrangements, called somatic hypermutation (SHM) and class switch recombination, aimed to produce Igs with the same antigen specificity, but improved affinity and different effector functions (IgG, IgA, IgE) (Stavnezer et al, 2008), allowing for a more effective and long lasting protection.

The main responsible of the genetic alterations at the B cell receptor locus is the DNA-editing enzyme activation-induced cytidine deaminase (AID). This protein, whose expression is induced in B cells by antigenic stimulation, converts deoxycytidine to deoxyuridine, generating mismatches between deoxyuridine and guanine that activate the error-prone mechanisms of DNA

repair. In this way, point mutations or indels are introduced in the site of deamination during B cell division with a frequency that is 10^5-10^6-fold higher than the mutation rate which normally occurs during DNA replication. These mutations fall in the sequences encoding for the heavy and light chain variable regions, with mutation hotspots in the complementarity-determining regions (CDRs), i.e. the short amino acid loops directly contacting the antigen (Di Noia et al, 2007; Maul et al, 2010). Only a small fraction of these mutations (about 20%) affects affinity; the B cells expressing Igs with lower affinity for the antigen die for apoptosis (a process called negative selection) due to the lack of antigen binding, which represents the stimulus for their survival and proliferation. On the contrary, the B cells in which a high affinity Ig has been generated by SHM are positively selected for proliferation and differentiate into antibody-secreting plasma cells or long-living memory B cells; alternatively, they undergo another cycle of mutagenesis in order to further increase Ig affinity as the immune response goes on (Gatto et al, 2010). The *in vivo* affinity maturation is able to generate antibodies with affinities in the picomolar range (10^{-10} mol/L) (Batista et al, 1998; Foote et al, 1995) (fig. 1).

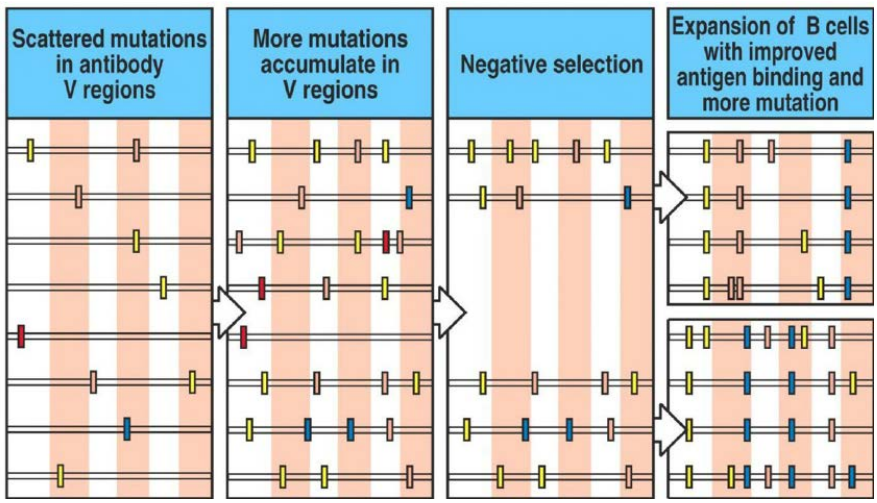

Fig. 1: schematic representation of *in vivo* antibody affinity maturation. Pink stripes represent the CDRs of the VH or VL, whereas colored bars indicate point mutations. At the beginning of the B cell response, they are interspersed throughout the variable region; while the immune response goes on, more mutations accumulate in this locus, but only B cells in which they increase the antibody affinity for the antigen can survive. Mutations are more frequent in the CDRs.

1.3. In vitro antibody affinity maturation

In vitro affinity maturation mimics the events that happen *in vivo*: the sequence of the lead antibody variable region is randomly mutated to generate a highly diversified *repertoire* of antibodies with different affinities for the same antigen; then the antibodies showing the highest affinity for the target are selected among this heterogeneous population. These *in vitro* technologies have successfully generated antibodies with low picomolar or even femtomolar affinities for their target (from 10^{-10} to 10^{-15} mol/L) (Boder et al, 2000). The most common approaches to generate these antibody repertoires starting from the parental sequence are random mutagenesis, randomization of targeted residues using degenerate oligonucleotides, chain shuffling and *in silico* approaches.

The random mutagenesis allows the generation of a broad range of variants of the parental antibody in which each residue could be potentially mutated; mutations are introduced through error-prone PCR or *E. coli* mutator bacterial strains, which are defective in DNA repair (Rasila et al, 2009).

The error-prone PCR (ep-PCR) has the advantage to select for a specific antibody region in which mutations have to be introduced; the mutagenesis can be targeted to the whole variable region or only to VH or VL or to more restricted sequences, most commonly one or more CDRs. The ep-PCR system is based on an error-prone Taq polymerase which, lacking proofreading activity, randomly inserts point mutations in the target sequences with high frequency. Nevertheless, at the amino acid level not all the substitutions have the same chance to occur at any position; this happens when two or even all the three nucleotides of the same codon have to be changed simultaneously to encode for a given amino acid (Neylon, 2004).

Randomization of targeted residues exploits degenerated oligonucleotides and restricts the mutagenesis only to specific amino acid residues. The target positions, generally identified by alanine-scanning, are modified with a series of *ad-hoc* PCR primers, in order to generate all possible amino acid substitutions (Ko et al, 2015).

Chain shuffling consists in combining a *repertoire* of VH with a fixed VL (or *vice versa*), but chain shuffling of the CDRs only are also described (Yoshinaga et al, 2008; Marks, 2004). In more recent works, *in silico* approaches have also been successfully used; these methods are based on computational design and structure predictions of antibody-antigen interactions (Clark et al, 2006; Barderas et al, 2008).

Once new *repertoires* have been generated, the antibodies with improved affinity can be selected by means of display methods, which are grouped into cell-based and cell free systems.

In cell-based approaches, the sequence variants of the parental antibody are showed (displayed) on the cell surface of yeasts (yeast surface display), phages (phage display), bacteria *(E. coli* surface display) or mammalian cells (commonly HEK293, CHO or B-lineage cells) (Doerner et al, 2014). The antibodies are fused to a proper protein of the cell surface and subsequently panned against the antigen of interest, provided in the format of soluble protein or in the mammalian cell surface context (whole cells or detergent-solubilized cell membranes) (Tillotson et al, 2013), if it is a membrane protein. Various cycles of panning are usually performed (up to 4 or 5), increasing the stringency of selection at each round in order to isolate and enrich the clones displaying the antibodies with the improved affinity; the stringency can be typically increased by a reduction of the antigen concentrations (Chao et al, 2006;). However, in some cases only one selection step has been sufficient to isolate high affinity variants.
The scFvs are the most commonly displayed antibody format due to their little size and the absence of post-translational modifications, which allows the production and display both in prokaryotes and eukaryotes. Fab fragments or full length Igs can be also displayed and in the case of whole antibodies, which need for post-translational modifications, eukaryotic systems are necessarily required (Doerner et al, 2014).
In cell free systems, which include ribosome display and mRNA display, the library generation is achieved by *in vitro* translation of the DNA, using ribosome preparations instead of the cellular translation machinery; chaperones and other enzymes are added to the reaction to help the proper polypeptide folding (Lipovsek et al, 2004).

1.4. Affinity maturation by yeast surface display (YSD)

YSD is the most widely used affinity maturation platform, combining a lot of advantages compared with the other methods (Chao et al, 2006; Gera et al, 2013). Firstly, unlike phages and bacteria, yeasts are eukaryotic cells, consequently the displayed proteins are properly folded by the endoplasmic reticulum chaperones and receive all the post-translational modifications necessary for their function.
In addition, the generation of the libraries is easier compared to all the other systems because it is achieved by *in vivo* yeast recombination, which is more efficient than *in vitro* cloning by ligation, used in the other display systems. Once generated by mutagenesis, the sequence variants are co-transformed with a proper yeast expression plasmid, which remains episomal after recombination. By optimization of the vector-insert ratio, a maximum transformation efficiency of about 10^9 colony forming units can be easily

obtained routinely (Benatuil et al, 2010), meaning that at most 10^9 different sequences can be found in a yeast library. Although, a higher theoretical diversity can be obtained by other approaches (up to 10^{11} by phage display or even 10^{14} by cell-free systems), a repertoire of 10^9 is considered more than enough when performing affinity maturation (Chao et al, 2006; Gera et al, 2013; Boder et al, 2000).

However, the main advantage of YSD is represented by the possibility to use flow cytometry to select for clones with improved affinity. The use of fluorescence allows a real-time quantification of the protein expression level and the antigen binding strength directly during the screening process. This detection method is very powerful to discriminate even little differences in the binding properties of the antibody variants.

Saccharomyces cerevisiae and, more recently, *Pichia pastoris* are the most commonly used species for YSD. Various yeast cell wall proteins are suitable as anchors for display, in particular the a- and α- agglutinins, the flocculin Flo1p and the Pir family proteins (Pir1-4) (Pepper et al, 2008). The most frequently used yeast strain is called EBY100; it has been generated through the genetic engineering of the chromosome of *S. Cerevisiae* BJ5465 strain and its display system is based on the a-agglutinin Aga (Chao G et al, 2006). Aga is a yeast mating protein with a dimeric structure, in which one subunit (Aga1p) is covalently linked to the cell wall through a glycosylphosphatidylinositol (GPI) anchor, while the other one (Aga2p) is linked to Aga1p by two disulfide bonds (fig. 2). Aga1p sequence is stably integrated into the yeast genome, whereas Aga2p gene is encoded by the episomal display plasmid and it is fused in frame with the antibody encoding sequences, at either their N or C-terminus; both Aga1p and Aga2p-antibody expression is driven by a galactose-inducible promoter; this system allows a fine tuning of the display level, up to $5x10^4$ molecules/cell. EBY100 genome has also been modified through the insertion of mutations in some genes involved in the synthesis of certain nucleotides and amino acids, rendering this strain unable to grow in absence of these substrates (the so-called auxothrophic strains). These missing proteins are provided by the plasmid used for recombination, consequently only yeasts in which the recombination has occurred are positively selected for growth in a medium deprived of the above nutrients.

The yeast-antigen complexes are detected using a two-color labeling with fluorescent antibodies (fig. 2 and 3) (Chao et al, 2006). One antibody (fluorescence 1, FL1 in fig. 2 and 3) recognizes a tag located at the N or C-terminus of the Aga2p fusion proteins expressed on yeast surface; therefore, this antibody is used to distinguish the displaying yeasts from the non-displaying ones that will appear as two distinct cell populations (a positive and a negative one, respectively) in a typical flow cytometry dot plot (lower

right and lower left quadrant, respectively, in fig. 3). As result, the fluorescence intensity of the displaying yeasts depends on how many Aga-antibody fusion proteins are showed on their surface. The advantage of using a C-term tag is that only yeasts displaying full length molecules can be detected and then included into the selection. The second antibody (fluorescence 2, FL2 in fig. 2 and 3) recognizes the soluble antigen or a surface marker of the antigen expressing cells. As a result, the displaying yeasts that bind the antigen are positive for both the fluorescences (upper right quadrant in fig. 3). Also in this case, the number of antigen molecules bound to each cell determines its fluorescence intensity in FL2 channel.
Fluorescence-activated cell sorting (FACS) is used to isolate the best binder yeasts. The cells of interest are identified directly on the plot before the isolation, by drawing a diagonal gating in the quadrant of the double positive fluorescent population (Gera N et al, 2013) and then sorted for the separation from the library. The diagonal gate should include those yeast clones that, for each level of scfv display along the abscissa, bound the highest number of antigen molecules (fig. 3).
The enrichment of the yeasts with a better antigen binding compared with the parental antibody is obtained through repeated sortings, typically three to five, in which the selection stringency is progressively increased using lower antigen concentrations at each selection step (Chao et al, 2006).

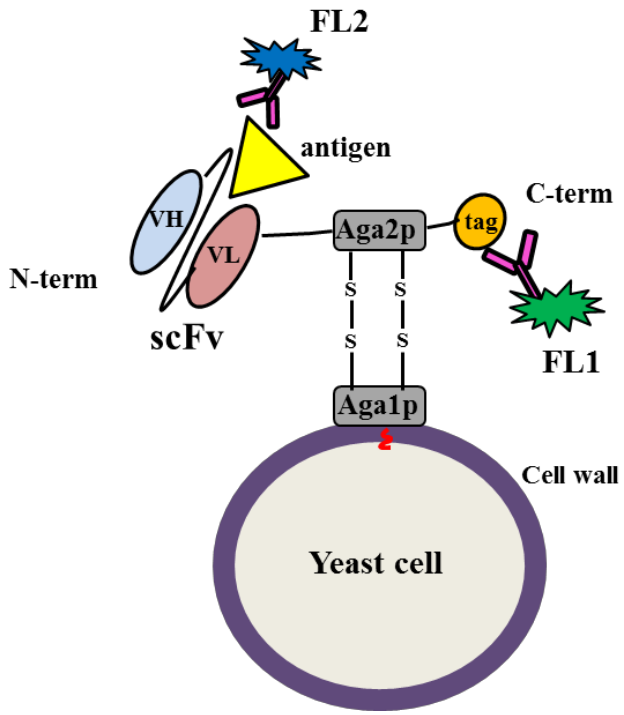

Fig. 2: Schematic representation of the detection system of the scfv-antigen complex by flow cytometry. The scfv is fused to the Aga2p subunit (at its N-terminus in this case) and this fusion protein carries a terminal tag (an example of a C-term tag is shown, in orange). The chimeric protein is covalently linked to Aga1p through two disulfide bonds and anchored to the yeast cell wall (purple) thanks to Aga1p GPI anchor (showed in red). The protein display is detected by an anti-tag fluorescent antibody (FL1). If the scfv binds to the antigen (in yellow), the complex is labelled with a second antibody (FL2), giving double fluorescent signal that can be detected by flow cytometry.

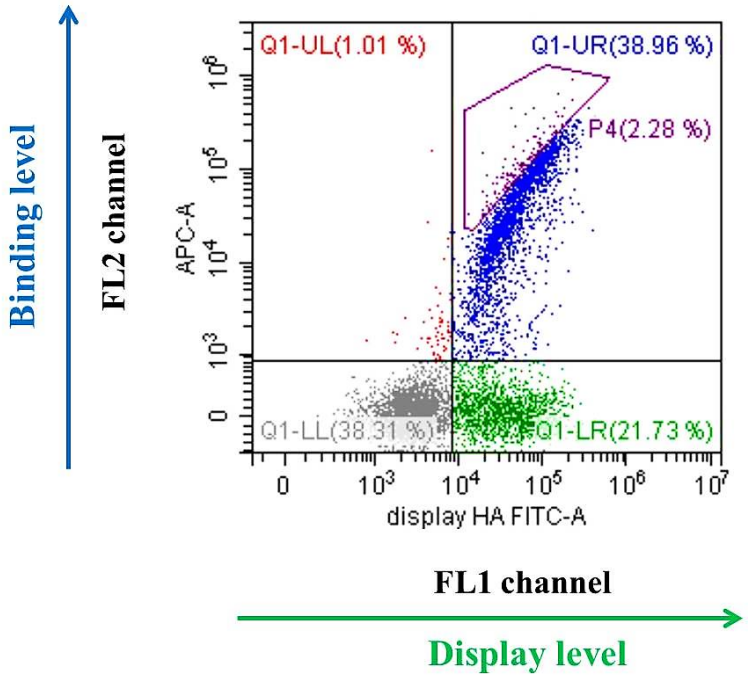

Fig. 3: typical flow cytometry dot plot in a YSD experiment. This example refers to a yeast library labelled with the two antibodies indicated in fig. 2 (FL1 and FL2) and shows the different cell populations (here represented by different colors), distinguished on the basis of their fluorescence level. Antigen binding cells are in the double positive quadrant (blue, Q1-UR quadrant) and are sorted by a typical diagonal gating strategy, here represented by the diagonal P4 gate (purple). In Q1-LR (single positive for FL1) displaying cells unable to bind the antigen are located, while the non-displaying yeasts appear in the double negative quadrant (grey, Q1-LL).

1.5. Antibodies with potential therapeutic application, isolated by YSD

A lot of examples of antibody affinity engineering through yeast display are reported in literature. The most surprising result is that obtained by Boder et al in 2000. They isolated some anti-fluorescein antibody fragments with an affinity of 48 fM, starting from a parental scFv with an affinity of 0,7 nM. These scFvs were isolated after four subsequent cycles of affinity maturation from libraries with complexities between 10^5 and 10^7. Their affinity is the highest so far reported for an engineered protein, but they are not for clinical use.

One of the most recent studies regarding antibodies for potential therapeutic application was performed in 2012 by Tillotson et al to improve the affinity of a scFv targeting the transferrin receptor. Since this is a plasma membrane protein, detergent-solubilized membranes of HEK293 cells, ectopically expressing this receptor, were used as source of the antigen. A library of about 5x10^7 yeast cells was generated by random mutagenesis of the whole parental scFv and its screening led to the identification of various scFvs with 3- to 7-fold improved affinities (from 0,38 to 0,18 nM) compared with the starting one.

By yeast display, antibodies against some toxins have been engineered too, such as botulinum neurotoxin type A (Siegel et al, 2005). After a single cycle of error prone mutagenesis of two previously identified anti-toxin scFvs (Kd values of 0,8-0,9 nM), two mutants were identified with 45- and 37-fold improved affinities, respectively (20 pM).

In 2005 Rajpal et al succeeded in generating improved versions of adalimumab (Kd 1 nM), an anti tumor necrosis factor-α (TNF-α) antibody already approved for the treatment of rheumatoid arthritis. They generated yeast libraries by applying a sort of high-throughput mutagenesis involving all the residues of the six CDRs; in this way, they isolated novel variants whose affinities were between 500- and 870-fold higher than adalimumab. Remarkably, these scFvs showed a 15- to 30-fold improvement of *in vitro* TNF neutralization.

Yeast display has been successfully used to improve affinity of a lot of proteins other than antibodies, such as T cell receptors (Buonpane et al, 2007; Buonpane et al, 2005), integrin I domain (Jin et al, 2006), epidermal growth factor (Cochran et al, 2006), natural killer cell receptor (Dam et al, 2003) and interleukin-2 (IL-2) (Rao et al, 2004). Affinity maturation is not the only application of YSD: its versatility has been also demonstrated in *de novo* selection of binders with specificity for a given target, epitope mapping, screening of cDNA libraries, identification of protein variants with improved production and stability (Pepper et al, 2008).

1.6. Antibodies in cancer treatment

Among all the FDA approved mAbs, many are used for cancer treatment, where they offer a variety of therapeutic solutions, being administered alone ("naked antibodies") or as immunoconjugates (Carter, 2001, Chiavenna et al, 2017).
Naked antibodies are used to mask the ligand-binding site or the dimerization site of oncogenic receptors, thus preventing their activation. In addition, some antibody isotypes (IgG1 and IgG3) are also able to activate the antibody-dependent cellular cytotoxicity (ADCC) and the complement-dependent cytotoxicity (CDC). These mechanisms involve natural killer (NK) cells and complement components, which are recruited by the antibody Fc effector domain on the cancer cell surface, inducing cell lysis (Clynes et al, 2000).
The immunoconjugates are widely used to deliver other therapeutic molecules or compounds only to cancer cells, limiting or avoiding the off-target effects of traditional chemotherapies which often damage healthy cells too (fig. 4). The immunoconjugates commonly vehicle cytotoxic molecules (toxins or radioactive isotopes), cytokines, killer cells or liposomes loaded with other drugs. They often carry enzymes which convert a prodrug in a toxic compound directly on cancer cell surface; alternatively, they are streptavidin-conjugated and used to capture a biotin-conjugated radioisotope only at the tumor site (multistep targeting).
A similar principle is used for the retargeting of oncolytic viruses; through genetic manipulation, some molecules of the viral envelope, which are involved in the recognition of normal cells, are replaced by tumor-specific antibody fragments, enabling the viruses to infect and lysing only tumor cells (Campadelli-Fiume et al, 2016).
Besides all these approaches, aimed to a direct destruction of cancer cells, an innovative antibody-based approach has emerged, whose purpose is to "awaken" the patient's immune system to fight cancer. A deeper understanding of cancer biology has brought to light that tumor cells have developed a lot of strategies to block the immune surveillance, resulting in tumor growth and progression and so explaining the resistance to the traditional therapies (Dunn et al, 2002).

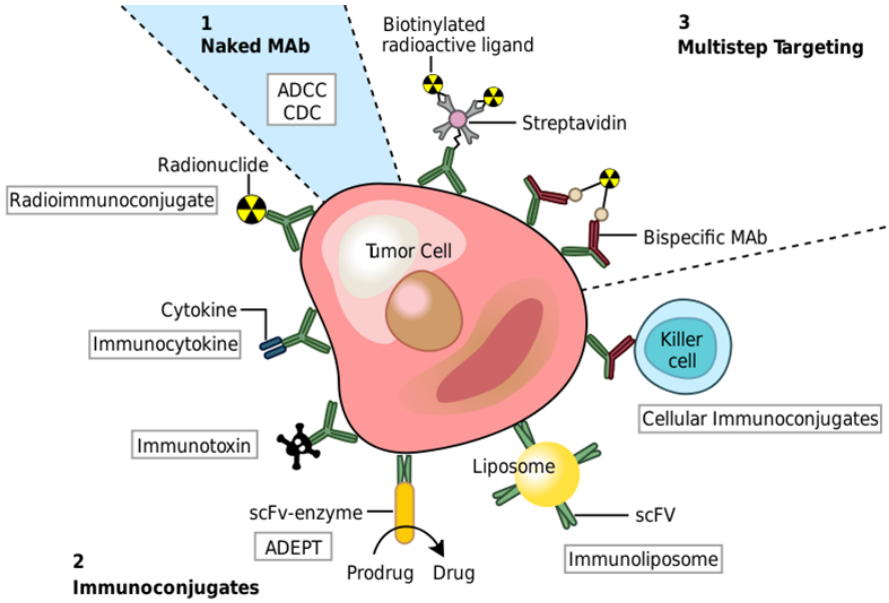

Fig. 4: applications of monoclonal antibodies in cancer treatment. In conventional anti-cancer treatments, mAbs are used alone (naked mAbs), to block oncogenic receptors and to activate antibody-dependent cellular cytotoxicity (ADCC) or complement-dependent cytotoxicity (CDC). Alternatively, mAbs are used to carry a variety of toxic compounds with non-specific activity only to tumor cells. ADEPT: Antibody-directed enzyme prodrug therapy.

1.7. Role of the immune surveillance in cancer progression and development of immune escape mechanisms

The cancer immune surveillance is the mechanism used by the immune system to recognize and remove cancer cells from our body; it is activated by tumor-associated neoantigens that result from the accumulation of mutations in various genes, due to the high genomic instability of cancer cells (Lawrence et al, 2013). The neoantigens are presented on the cell surface in complex with the Major Histocompatibility Complex-class I (MHC I) and then recognized by T cells as non-self-antigens (Snyder et al, 2015; Sensi et al, 2006); as result, the adaptive immune system is activated in order to kill cancer cells.

Among the several strategies developed by tumors to escape the immune surveillance, the one arousing the greatest therapeutic interest is the upregulation of molecules that activate the immune checkpoints (Pennock et al, 2015), a group of pathways which suppress T cell functions. Considering that these molecules are showed on cancer cell surface, they can be easily blocked by mAbs and so they have become an attractive therapeutic target.
This is not the only strategy adopted by tumors to evade immunity. Another common escape mechanism is the impairment of the MHC I antigen presentation or of the endoplasmic reticulum and Golgi epitope processing, through genetic and epigenetic alterations (Fruci et al, 2012; Seliger et al, 2002). In fact, a reduced expression of proteins associated with the immunoproteasome, such as the subunits low-molecular-weight protein 2 and 7 (LMP-2 and LMP-7), or with the endoplasmic reticulum, for example the transporter associated with antigen presentation (TAP), has been reported in some tumors and cancer cell lines (Seliger et al, 1996; Alpan et al, 1996; Pandha et al, 2007).
At last, tumors can evade the immune system by secreting immunosuppressive mediators that are able to inhibit the maturation and/or activation of tumor infiltrating immune cells. These effects are mainly due to the constitutive activation of the signal transducer and activator of transcription 3 (STAT3) pathway observed in many cancers (Wang et al, 2004), which leads to the production of vascular endothelial growth factor (VEGF), IL-10, IL-6 and transforming growth factor-β (TGF-β) (Johnson et al, 2007; Liu et al, 2012). These molecules block NK and granulocyte effector functions, impair dendritic cell (DC) differentiation (Wang et al, 2004) and promote the commitment of immature myeloid cells into myeloid suppressor cells, i.e. a subset of cells that inhibit T lymphocyte functions (Gabrilovich et al, 2009; Gabrilovich et al, 2012).

1.8. The immune checkpoints - the PD-1/PD-L1 pathway and its role in the regulation of T cell functioning

The activity of T cells, which have a central role in the adaptive immunity against cancer, is regulated through a balance between activating and inhibitory stimuli generating from two different groups of surface receptors. The activating stimuli are also called co-stimulatory signals; they are necessary for activation of naïve T cells after the binding of the T cell receptor (TCR) to the MHC I-peptide complex. The co-stimulatory receptors are grouped into two main families. The first is the B7/CD28 family, which includes CD28, the inducible costimulator (ICOS) and the B- and T-lymphocyte attenuator (BTLA); among them, the best characterized receptor

is CD28, which is activated upon binding of B7-1 (CD80) and B7-2 (CD86) expressed on antigen presenting cells (APCs). CD28 co-stimulation leads to cell cycle progression and increases cell metabolism through the activation of PI3K/AKT pathway.
The other main group is the tumor necrosis factor receptor (TNFR) family. The members of this group, which includes CD40, CD27, CD30, OX40, 4-1BB and the glucocorticoid-induced TNFR-related gene (GITR), share a common T cell activation mechanism that is the stimulation of the nuclear factor-kB (NF-kB), with the consequent increase in expression of pro-inflammatory genes.
The signaling pathways that negatively regulate T cell function are called immune checkpoints and play a key role in two main mechanisms. The first is the peripheral tolerance (Fife et al, 2008), a process that blocks the self-reactive T cells that escape from negative selection in the thymus; the second is the switching-off of T lymphocyte effector functions that normally occurs during an immune response. This group of receptors includes the cytotoxic T lymphocyte-associated antigen 4 (CTLA-4), the programmed death-1 (PD-1) receptor, the lymphocyte-activation gene 3 (LAG-3) and the T cell immunoglobulin 3 (TIM-3); among them, CTLA-4 and PD-1 pathways are the best characterized ones.
CTLA-4 is expressed on T cells as a response to T cell activation and competes with the co-stimulatory receptor CD28 for the binding to the B7 ligand. CTLA-4 signaling is mediated by the intracellular phosphatase PP2A, which switches-off the Akt pathway, previously activated by co-stimulatory receptors.
PD-1 (also known as CD279) is a monomeric transmembrane protein of the Ig superfamily and its sequence shares 64% of homology with its murine orthologue (Lin et al, 2008). PD-1 extracellular region contains an IgV-like domain that interacts with the Ig domains of its ligands, programmed death ligand-1 and -2 (PD-L1 and PD-L2); the cytoplasmic tail has no intrinsic enzymatic activity but contains two tyrosine-based signaling domains, called immunoreceptor tyrosine-based inhibitory motif (ITIM) and immunoreceptor tyrosine-based switch motif (ITSM), whose tyrosine residues are phosphorilated and recruit PD-1 downstream effectors to the plasma membrane (Riley, 2009).
PD-L1 (also called B7-H1 or CD274) has 70% sequence identity with its murine orthologue, which allows *in vitro* cross reactivity between murine and human PD-1 and PD-L1 (Lin et al, 2008). Unlike its receptor, PD-L1 extracellular region contains two Ig domains, an N-terminal IgV-like domain that binds to PD-1 and an IgC-like one. It is a monomeric protein, but crystallographic analyses showed that it can exists in solution as dimeric complex too, although it is not clear the role of this complex *in vivo* in

immune system functioning (Chen et al, 2010). The other ligand PD-L2 (B7-DC or CD273) was discovered more recently than PD-L1 (Latchman et al, 2001). These two ligands have the same structure and share 40% amino acid identity.

All downstream effects of PD-1 are mediated by the Src homology phosphatase 2 (SHP-2), which is recruited *via* a Src homology 2 **(**SH-2) domain to the phosphorylated ITIM motif (Zhang et al, 2004). Among SHP-2 substrates, we find the lymphocyte-specific protein tyrosine kinase (Lck) and the zeta-chain-associated protein kinase 70 (ZAP-70), which are the main effectors of the TCR; they are inactivated through dephosphorilation by SHP-2, blocking the TCR signaling and consequently downregulating the target genes that promote T cell effector functions (Sheppard et al, 2004). PD-1 activation also impairs the PI3K/Akt and Ras/MAPK pathways (Parry et al, 2005), (fig. 5). The blockade of the PI3K/Akt pathway mainly affects glucose metabolism, by reducing the glycolytic enzyme activity and the expression of glucose transporters on T cell membrane; as a consequence, T cells are deprived of the main source of energy necessary for their growth and cell division. These metabolic changes also alter their differentiation (Chang et al, 2013; Patsoukis et al, 2015), promoting the switch from a T effector to a Treg and T-exhausted phenotype, which are responsible for the suppression of the immune response. On the other hand, the PD-1 mediated inhibition of the Ras/MAPK signaling, which is involved in the positive regulation of the cell cycle, stimulates T cells to enter G0 phase (Patsoukis et al, 2012); as a result, T cell proliferation is blocked.

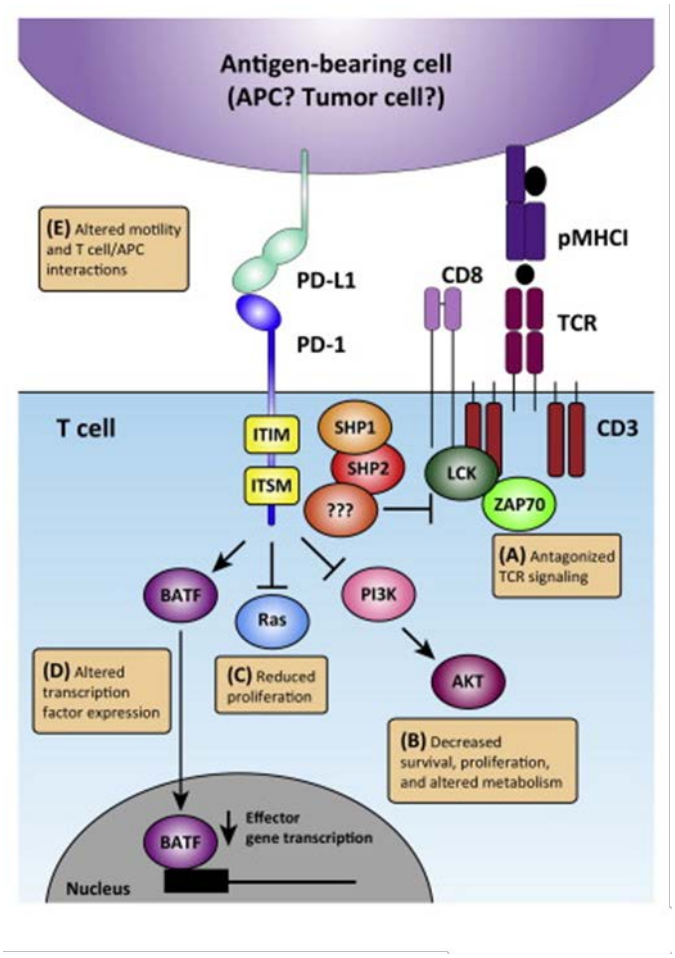

Fig. 5: schematic representation of PD-1 intracellular pathway. Upon engagement of PD-1 (in blue, on T cell surface) by PD-L1 (in light blue on APC or tumor cell surface), the SHP1/SHP2 phosphatases are recruited to PD-1 effector domains (in yellow) and then activated. These proteins affect the function of several targets: the complex of the T cell receptor (TCR, on the right), the Ras/MAPK and PI3K pathways and the basic leucine zipper transcriptional factor ATF-like (BATF). Boxes A, B, C, D and E summarize the resulting molecular and cellular alterations.

1.9. Impairment of PD-1/PD-L1 pathway in cancer

PD-1 expression is limited to immune cells, both lymphoid and myeloid lineages (T and B lymphocytes, NK cells, monocytes and DCs) (Keir et al, 2008), in which it is expressed at a low basal level. During the immune response, it is upregulated by the cytokines IL-2, IL-7, IL- 15, IL-21 and interferon-α (IFN-α) (Kinter et al, 2008; Cho et al 2008) and by a prolonged stimulation of T and B cell receptors (Freeman et al, 2006).
On the contrary, PD-L1 expression is not restricted to immune cells; in healthy conditions, it is expressed in many other tissues to protect themselves from immune attacks; PD-L1 is found at high levels in thymus cortex, lung, heart muscle, placenta, liver, mesenchymal stem cells and vascular endothelium; lower PD-L1 levels are found in pancreatic islets, astrocytes, neurons, keratinocytes (Keir et al, 2008), cornea and retina (Hori et al, 2006; Sugita et al, 2009). A lot of cytokines produced during the immune response, such as IL-2, IL-10, IL-7, IL-15, IL-21 and IFN-γ, upregulate PD-L1 in immune cells.
Interestingly, PD-L1 is expressed at high levels in many kinds of hematologic and solid tumors, due to the constitutive activation of some oncogenic pathways that positively control its transcription, in particular STAT3 (Marzek et al, 2008), PI3K/Akt and PI3K/mTOR pathways (Crane et al, 2009). Moreover, the IFN-γ present in the tumor microenvironment can induce PD-L1 expression too. IFN-γ is secreted by tumor infiltrating T lymphocytes activated by tumor antigens during the early stages of cancer development; in addition to its pro-inflammatory activity, this cytokine upregulates PD-L1 in tumor cells and so it is responsible for the suppression of T cell antitumor activity (fig. 6) (Taube et al, 2012). High PD-L1 levels have been detected not only on cancer cells, but also on the surface of the immune and non-immune cells that form the tumor microenvironment, that is macrophages, DCs, stromal fibroblasts and the endothelium of tumor neovasculature (fig. 7).

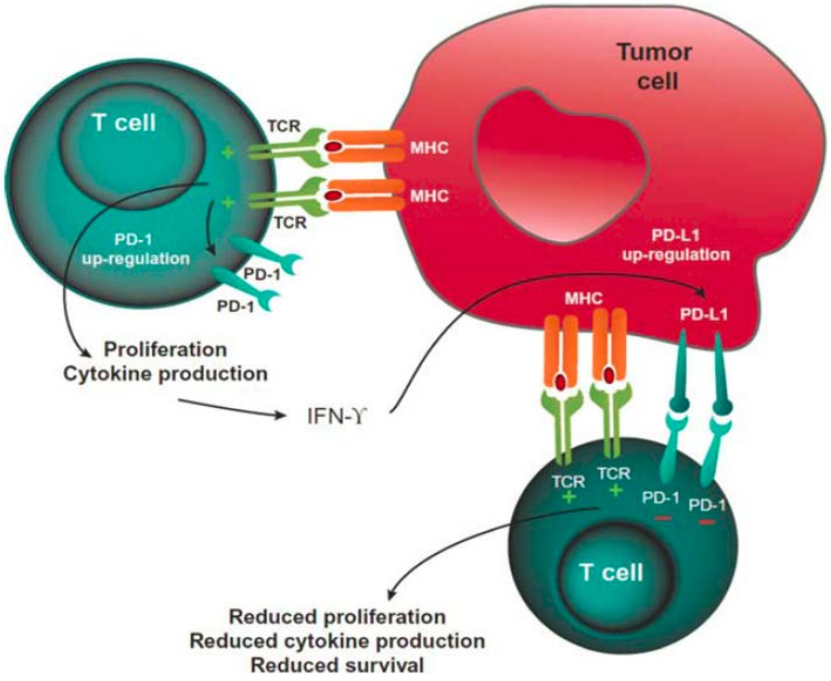

Fig. 6: mechanism of PD-L1 mediated inhibition of T cells by tumors. T cells activated by tumor- specific antigens, proliferate and produce cytokines. These inflammatory stimuli upregulate PD-L1 in tumor cells; its binding to PD-1 expressed on the same T cells negatively regulate their proliferation and effector functions, preventing cancer cells from killing.

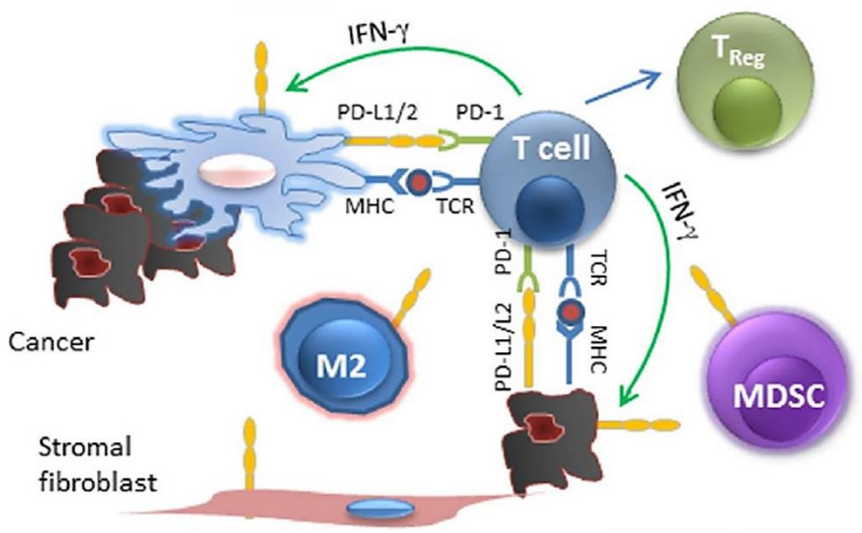

Fig. 7: PD-L1 and PD-L2 expression in the tumor microenvironment. Cancer cells (in black), stromal fibroblasts, tumor-infiltrating myeloid-derived suppressor cells (MDSC) and macrophages (particularly M2 subtype) show PD-1 ligands on their surface (in orange). This promotes the engagement of infiltrating T lymphocytes and their differentiation into Treg cells, with immunosuppressive activity.

PD-L2 is expressed only on stromal cells of thymus medulla, macrophages, bone marrow derived mast cells, peritoneal B1 cells and activated DCs (Zhong et al, 2007). In DCs its expression is positively regulated by IL-4 and granulocyte-macrophage colony-stimulating factor (GM-CSF) (Selenko-Gebauer et al, 2003). PD-L2 is also expressed in various types of human tumors (Rozali et al, 2012); however, it has not received as much attention as PD-L1 and its role in modulating antitumor immunity is less clear.
The overexpression of PD-L1 on cancer cells (or cells of the tumor stroma) is used by tumors as a mechanism of escape of the immune response, to protect themselves from killing by T cells. The binding of PD-L1 to its receptor PD-1 expressed on the tumor infiltrating lymphocytes activates the PD-1 checkpoint, blocking the downstream T cell pathways involved in cytotoxic response against the tumor.
The binding of PD-L1 to PD-1 is able to transduce signals not only in T cells, but in cancer cells too (Azuma et al, 2008). In fact, PD-L1 can act as PD-1 receptor in tumor cells, transmitting them anti-apoptotic signals which

enhance their resistance to apoptosis induced by both immune effectors and proapoptotic drugs.

1.10. Targeting of immune checkpoints with mAbs

Considering that the activation of immune checkpoints is a common mechanism used by tumors to escape the immune surveillance, there has been a great interest in developing therapeutic strategies that blocked these pathways. A great promise for cancer treatment is represented by the monoclonal antibodies that recognize the checkpoint receptors or ligands, preventing them to bind to each other. In this way, the inhibitory signals transduced to immune cells are blocked, so that they are reactivated to recognize and kill tumor cells (fig. 8).

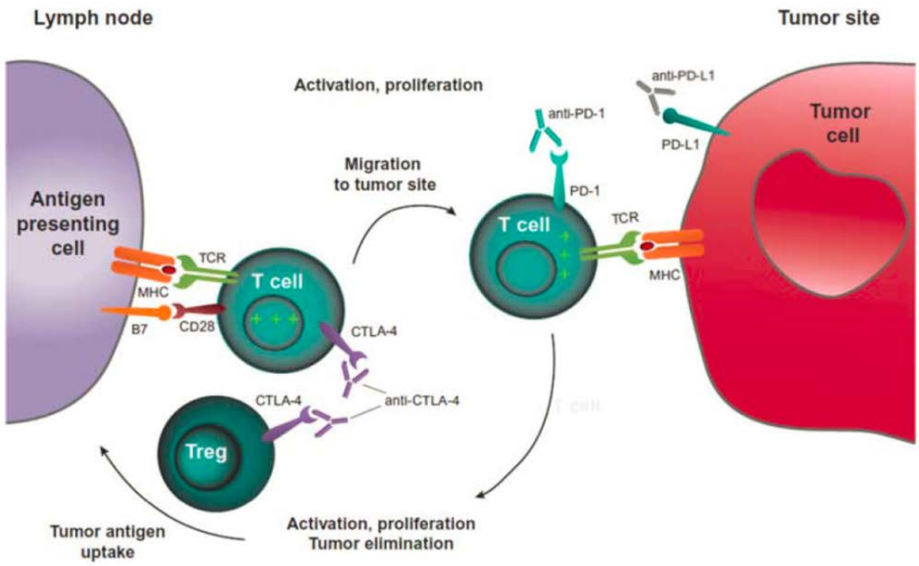

Fig. 8: effects of the immune checkpoint blockade by monoclonal antibodies. The binding of therapeutic mAbs to immune checkpoint components (anti CTLA-4, anti PD-1 and anti PD-L1, in purple, light blue and grey, respectively) removes the negative stimuli to T cell proliferation. In this way, T cells are re-activated to proliferate and recognize cancer cells. If used in combination, these antibodies can have a sinergistic effect.

A lot of monoclonal antibodies have been designed to target components of both activating and inhibitory pathways for the treatment of many solid tumors and hematologic malignancies (Peggs et al, 2009) (fig. 9). Many of these mAbs are in different phases of clinical development, few others have already been approved by FDA. The most targeted checkpoints are CTLA-4 and PD-1.

Ipilimumab, an anti CTLA-4 IgG1, was the first checkpoint inhibitor approved by FDA; it entered clinics in 2011 in USA and Europe for the treatment of unresectable or metastatic melanoma (Wolchok et al, 2013). Other clinical trials are ongoing for the evaluation of its therapeutic efficacy in combination regimens with other checkpoint inhibitors, in advanced melanoma cases which had not received any previous treatment (Larkin et al, 2015; Hodi et al, 2016). Ipilimumab, in combination with chemotherapy or other mAbs, is in advanced clinical trial also for the first line treatment of other solid tumors, particularly small and non-small cell lung cancer (SCLC and NSCLC) (Lynch et al, 2012; Reck et al, 2013; Antonia et al, 2016).

Given the therapeutic success of CTLA-4 blockade, other checkpoints have been targeted, particularly the PD-1/PD-L1 checkpoint. Among the antibodies developed to target this pathway, pembrolizumab and nivolumab have already been approved by FDA, while the others are in advanced clinical trials.

Pembrolizumab, a humanized IgG4, was the first anti PD-1 mAb to be approved by the FDA in 2014 for the treatment of metastatic melanoma that was not responsive to previous treatment with ipilimumab or with BRAF inhibitors (in tumors with BRAF mutations) (Robert et al, 2015). In 2015, the FDA extended its approval also to NSCLC (Garon et al, 2015).

Nivolumab is a fully human IgG4 in clinical use for the treatment of melanoma since 2014, with the same therapeutic indications as pembrolizumab (Weber et al, 2015). It demonstrated a good response rate in both untreated and previously treated metastatic melanoma cases. Very good results were obtained when nivolumab was used in combination with ipilimumab; in fact, in a phase III trial, the group of advanced melanoma patients treated with both the antibodies showed a 5-fold higher response rate than the group treated with ipilimumab alone (Postow et al, 2015). The clinical efficacy of nivolumab was also proven in squamous and metastatic NSCLC, renal cell carcinoma (RCC), head and neck cancer and Hodgkin lymphoma; in this last case the response rate was even 87% (Ansell et al, 2015).

Interestingly, a higher clinical response rate to these two anti PD-1 mAbs was observed when tumors expressed high levels of its ligand PD-L1 (Weber et al, 2015). The same result was also obtained after treatment with MPDL3280A (atezolizumab), a human anti PD-L1 IgG1 that was tested on

277 patients affected by various types of advanced incurable cancer (NSCLC, melanoma, RCC, colorectal cancer, gastric cancer and head and neck squamous cell carcinoma) (Herbst et al, 2014). Tumors that upregulated PD-L1, especially on tumor infiltrating immune cells, showed a better response than those tumors in which no or very low PD-L1 levels were detected. This studies support the hypothesis that PD-L1 expression within the tumor could be considered as a predictive biomarker of good outcomes upon treatment with PD-1/PD-L1 inhibitors.

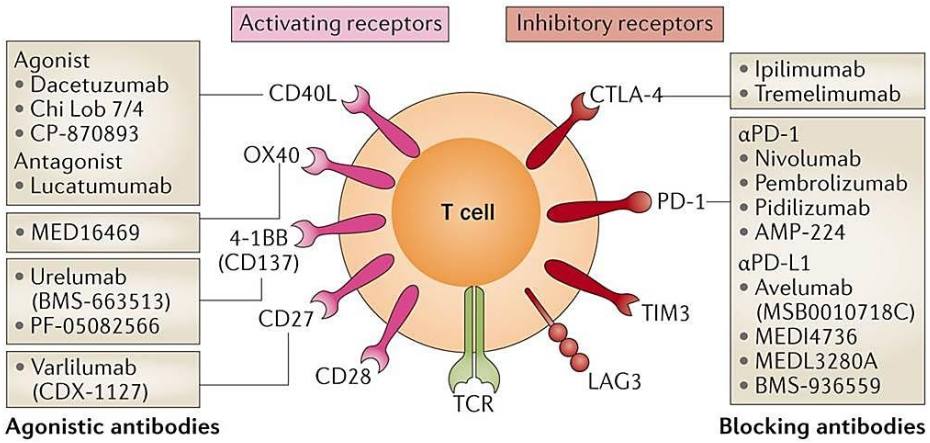

Fig. 9: spectrum of mAbs developed against activating or inhibiting T cell surface receptors to reactivate the antitumor immune response.

2. AIM

The aim of this study is the generation of novel and high affinity anti PD-L1 antibody fragments through a yeast surface display affinity maturation approach exclusively targeted to the complementarity-determining region 3 (CDR3) of the heavy chain variable region (VH).
PD-L1 is a component of the PD-1/PD-L1 immune checkpoint pathway, which is involved in the blockade of T lymphocyte activation. PD-L1 is overexpressed in many human tumors, with the consequent inhibition of the T cell-mediated antitumor immunity. The blockade of the PD-L1 mediated signaling with monoclonal antibodies represents a promising approach in cancer immunotherapy.
The yeast surface display technique relies on the construction of single chain variable fragment (scFv) mutant libraries and the screening for clones with improved antigen affinity by Fluorescence Activated Cell Sorting (FACS).
In particular, this work has the purpose to set up an improved and faster protocol focusing on both the mutagenesis and screening steps.
The optimal CDR3-targeted mutagenesis conditions will be identified, in order to generate yeast libraries with high mutant frequency and diversity; moreover, concerning the screening process, a selection scheme will be developed which easily excludes the wild type scFv clones and rapidly leads to an enrichment of mutants with improved affinity.

3. MATERIALS AND METHODS

3.1. Cell lines and culture media

The Human embryonic kidney EBNA 293 (Invitrogen, Thermo Fisher, Waltham, Massachusetts, USA) were used as host cell line to express the full length IgGs. The EBNA 293 cells stably express the Epstein Barr Nuclear Antigen 1 (EBNA-1) gene, encoding for a protein that is responsible for episomal replication and maintainance of oriP-containing plasmids. EBNA 293 cells were grown in Dulbecco's Modified Eagle Medium (Gibco, Thermo Fisher Scientific, Waltham, Massachusetts, USA), supplemented with 10% (v/v) heat-inactivated Fetal Bovine Serum (FBS, Sigma-Aldrich, Saint Louis, Missouri, USA), 2mM L-glutamine (Gibco), 100U/ml penicillin and 100 µg/ml streptomicin (Gibco), 250 µg/ml Geneticin (G418 sulphate, Gibco). They were cultured at 37°C in a humidified atmosphere with 5% CO_2.
The human peripheral blood mononuclear cells (hPBMCs) isolated from healthy donors were cultured in RPMI 1640 medium (Gibco), supplemented with 10% (v/v) heat-inactivated FBS (Sigma), 2mM L-glutamine (Gibco), 100U/ml penicillin and 100 µg/ml streptomicin (Gibco), HEPES 10mM (Gibco), and grown at 37°C in a humidified atmosphere with 5% CO2.

3.2. Bacterial strains and culture media

Chemically competent *E.Coli* DH5α (Invitrogen) were used for the amplification of all plasmids (see plasmids) and for transformation of the topo cloning reactions. The high efficiency chemically competent *E.Coli* DH10B cells (Invitrogen) were transformed with plasmid DNA extracted from yeast cells.
Luria-Bertani (LB) culture medium, prepared as described by Sambrook et al in 1989, was used for bacteria's growth. The selection of transformants was done by adding 100 µg/ml ampicillin (Applichem, Darmstadt, Germany) to LB medium, both liquid and semisolid.

3.3. Yeast strains

The *S. Cerevisiae* strain EBY100 (ATCC) was used to generate all the scFv-displaying yeasts (libraries and to single yeast clones isolated from the sortings). EBY100 is derived from the *S. Cerevisiae* BJ5465 strain by a genomic insertion of the gene encoding for the a-agglutinin subunit Aga1p,

whose expression is controlled by the galactose-inducible GAL1 promoter. EBY100 is a MATa strain and carries the following auxotrophic mutations: *ura352 , trp1, leu2delta200, his3delta200, pep4HIS3, prbd1.6R, can1, GAL*. *TRP1* (a gene involved in tryptophan biosynthesis, containing an amber mutation) was used as selection marker to isolate all the transformed yeasts.

3.4. Yeast culture media

The EBY100 yeast strain was grown in rich non selective medium YPD (Yeast-Peptone-Dextrose). The transformed EBY100 yeast cells were cultured in the selective medium Yeast Nitrogen Base -tryptophan (YNB -trp). To allow the display of scFvs on the yeast surface, EBY100 transformants were grown in the YNB induction medium. The composition of all liquid and semisolid culture media is reported in table 1.

yeast culture media and solutions	composition	notes	supplier
YPD	deionized water	autoclaving at 121°C for 20’	
	10g/L yeast extract		sigma
	20g/L peptone		sigma
	20g/L agar (only for semisolid medium)		sigma
	2% D-glucose	freshly added after autoclaving	
	100U/ml penicillin and100 µg/ml streptomicin		gibco
selective medium YNB	deionized water	autoclaving at 121°C for 20’	
	6,8 g/L yeast nitrogen base		sigma
	20g/L agar (only for semisolid medium)		sigma
	2% D-glucose	freshly added after autoclaving	
	1X yeast synthetic drop out without tryptophan		
	100U/ml penicillin and100 µg/ml streptomicin		gibco
induction medium	deionized water	autoclaving at 121°C for 20’	
	6,8 g/L yeast nitrogen base		sigma
	0,05% D-glucose	freshly added after autoclaving	
	2% D-galactose		
	1X yeast synthetic drop out without tryptophan		
	100U/ml penicillin and100 µg/ml streptomicin		gibco
20% D-glucose stock solution	deionized water	0,22 µm filtration	
	200g/L D-glucose		sigma
20% D-galactose stock solution	deionized water	0,22 µm filtration	
	200g/L D-galactose		sigma
10X yeast synthetic drop out without tryptophan stock solution	deionized water	0,22 µm filtration	
	19,2g/L yeast synthetic drop out without tryptophan		sigma

Table 1: yeast culture media and solution recipes and instructions for their preparation.

3.5. Plasmids

The pYD1 plasmid (Invitrogen) was used for the scFv expression. This vector contains an expression cassette including the AGA2 gene, under the control of GAL1 promoter, and a multiple cloning site for the cloning of the gene of interest; this system allows an inducible, galactose-driven expression of the protein of interest on the yeast cell surface, in fusion with Aga2p subunit of the a-agglutinin Aga (data sheet). In addition, this plasmid carries the TRP1 gene (described above), used as selection marker for the transformed yeasts, and the ampicillin resistance gene. Two different origins of replication are present, for propagation into yeasts and bacteria, respectively.
The plasmid pYD1-D25-Aga2-HA, was generated by Geneart synthesis service (Thermo Fisher Scientific). The expression cassette, containing the GAL1 promoter and the sequence of the wild type scFv D25 in frame with Aga2p and HA tag at the 3' end, was *de novo* synthesized and then cloned into pYD1 using BtgZI and PmeI restriction sites. Moreover, in order to provide the highest possible display of the scFvs the codon usage of the cassette was optimized for expression in yeast system.
The plasmids pEU8.2 and pEU4.2 were used for expression of the mAbs in EBNA cells. These plasmids encode for the constant regions of the VH and VL of the IgGs type 4, respectively. To convert the scFvs into full-length IgGs type 4, the sequences of the VH and VL of each scFv were *de novo* synthesized by Geneart synthesis service with a human-optimized codon usage and then subcloned in frame with the respective constant regions. VH cloning in pEU8.2 was performed *via* BssHII and SalI restriction sites, while each VL was cloned in pEU4.2 *via* ApaLI and AvrII sites.

3.6. Bacterial transformation

The transformations were performed according to manufacturers' recommendations. Briefly, cells were incubated with DNA for 30 min on ice, then they were heat-shocked at 42°C for 40 sec and placed on ice again for 2 min. They were subsequently recovered in 500 µl SOC medium (Invitrogen) by shaking at 37°C for 30 min (only for circular plasmid) or 1 hour (in all other cases). Aliquots of each transformation reaction (1/5 and 1/10) were spread on separate LB plates with antibiotic selection and grown overnight at 37°C. Only for transformation of DH10B, all the cells were spread on the same plate.

3.7. Preparation of yeast competent cells

EBY 100 was streaked on an YPD plate and grown at 30°C for 36-48h. A single colony was inoculated in 5 ml of YPD and grown overnight at 30°C in a platform shaker until the stationary phase that corresponds to approximately 5-6 optical density (OD) at 600 nm (at this wavelength 1 OD of culture contains more or less 1x10^7 yeast cells/ml, Chao et al, 2006). 200 ml of YPD were then inoculated at 0,003 OD/ml with yeasts from the previous inoculum and grown overnight. When reached the mid-log phase, corresponding to 1,5-1,6 OD (after about 16h of growth at 30°C in a platform shaker at 200-250 rpm), yeast cells were harvested by centrifugation at 2000xg for 30 min at 4°C, washed twice with 25 ml of ice-cold filter-sterilized ultrapure Milli-Q water and once with Ice Cold Electroporation Buffer (ICEB: 1mM calcium chloride, 1M sorbitol, in Milli-Q water). After each washing, yeasts were centrifuged at 2000xg for 10 min at 4°C. Soon after, yeast cells were conditioned in 20 ml Lithium Acetate - dithiothreitol buffer (LAD buffer: 0,1M Lithium Acetate, 10 mM dithiothreitol, in Milli-Q water) for exactly 30 min at 30°C with gentle shaking (100 rpm). Competent yeasts were collected as before and, after 1x washing with ICEB, they were resuspended in the same buffer to reach a final volume of 1 ml and used immediately for library generation. ICEB and LAD buffer were prepared immediately before use and filter-sterilized.

3.8. Yeast transformation

3.8.1. Generation of scFv-displaying yeast libraries

To generate scFv-displaying yeast libraries, 1,3x10^9 yeast competent cells resuspended in 400 µl ICEB were mixed with the pYD1-D25-Aga2-HA vector and the randomly mutated scFv inserts with a 1:25 molar ratio. To allow *in vivo* recombination between the plasmid and the scFvs, pYD1-D25-Aga2-HA was firstly linearized with BtgzI and PmeI restriction enzymes (New England Biolabs, Ipswich, Massachusetts, USA) and 1µg of the purified plasmid was added to 8-9 µg of insert (not more than 40 µl of final volume). In order to reach a transformation efficiency of about 1-2x10^8 transformants, two different aliquots of competent yeast cells were electroporated separately.
Cells were then transferred to a pre-chilled electroporation cuvette with 2 mm electrode gap and after 5 minute incubation on ice, they were electroporated by using Gene Pulser Xcell™ (Biorad, Hercules, California, USA) according to the following exponential protocol: voltage 2500V, resistance 100 ohm,

capacitance 25 µF. After electroporation, each aliquot was immediately recovered in 8 ml of a 1:1 mix of YPD and 1M Sorbitol for 2h at 30°C, in a platform shaker at 200-250 rpm. The two aliquots of electroporated cells were therefore collected at 2000xg for 10 min at room temperature, pooled and resuspended in 200 ml of selective medium YNB trp-. The culture was grown for 16-20h at 30°C, in a platform shaker at 200-250 rpm. 20% (v/v) glycerol stocks were made, each containing a ten-fold excess of the expected library diversity.

3.8.2. Generation of individual scFv-displaying yeast clones

To obtain yeast clones expressing a single type of scFv, 3,2 x10^8 yeast competent cells, resuspended in 100 µl ICEB, were mixed to 30-40 ng of the circular plasmid pYD1-Aga2-HA, encoding for the scFv of interest. Cells were prepared as before and electroporated with MicroPulser (Biorad) using the preset protocol Sc2. After the recovery phase (the same as described for the generation of the libraries), yeasts were collected, resuspended in 100 ul of selective medium YNB trp- and plated on a single YNB trp- plates.

3.9. Determination of the transformation efficiency

To determine the transformation efficiency, that also corresponded to the theoretical library diversity, serial dilutions (1:100, 1:1000, 1:10000 and 1:100000) were prepared from libraries in selective medium and 100 µl of each dilution were spread on selective plates and grown at 30°C for 36-48h. The number of colony forming units (CFU) was counted and the titer was calculated as the average of the counts obtained for each plate.

3.10. Isolation of plasmid DNA from bacterial and yeast cultures

Plasmid DNA from bacterial cultures was extracted by QIAprep Spin Miniprep Kit and EndoFree plasmid maxi kit (both from Qiagen Hilden, Germany), according to manufacturer's recommendations. For the propagation of this DNA, 50 ng of the plasmid from these extractions were used to transform *E.Coli* DH5α cells.
For the extraction of good quality plasmid DNA from yeast cultures, the procedure was adapted from the QIAprep Spin Miniprep Kit Protocol with some modifications. In brief, 60 OD of fresh overnight cell culture were harvested at 2000xg for 10 min at 4°C and resuspended in 750 µl buffer P1.

500 µl of acid-washed glass beads (Sigma) were added to the cell suspension and the yeast cell wall was mechanically destroyed by the Tissue lyser (Qiagen) for 2 min at 30 Hz. Chemical lysis and subsequent neutralization were performed in 750 µl buffer P2 and N3, respectively. Lysate clarification and DNA binding to column were performed according to QIAprep Spin Miniprep Kit handbook. After washing with 500 µl buffer PB and 750 µl buffer PE, DNA was eluted in 30 µl UltraPure DNase/RNase-Free Distilled Water (Gibco) and its concentration was determined by a spectrophotometer at 260 nm. 200 ng of this plasmid DNA were used to transform 50 µl of DH10B cells.

3.11. Determination of scFv CDRs

The Complementary Determining Regions (CDRs) of the anti PD-L1 scFv D25 were identified by the Kabat system (Kabat, 1991), using the IgBLAST software.

3.12. Generation of repertoires of randomly mutated CDR3s

To generate *repertoires* of scFvs with improved affinities for the PD-L1 protein, the CDR3 of D25 scFv was randomly mutagenized using GeneMorph II Random Mutagenesis Kit (Agilent Technologies, Santa Clara, California, United States). 1 ng, 100 pg, 10 pg and 1 pg of pYD1-D25-Aga2-HA plasmid were used as template in four different error-prone CDR3 amplification reactions, with the following primers and reaction conditions: forward 5'-GAAGATACTGCTGTTTACTACTGTGCTAGA-3' (primer 1 in fig. 10); reverse 5'-CAGTAACCATAGTACCTTGACCCCA-3' (primer 2 in fig. 10); 30 sec denaturing at 95°C, 30 sec annealing at 60,3°C, 15 sec extension at 72°C, 30 cycles of amplification.
The 3' ends of the primers annealed with the bases immediately upstream and downstream the CDR3, respectively so that no nucleotide of the framework regions should be involved in the mutagenesis.
The template DNA possibly present in the amplification product was digested with 1 µl DpnI at 37°C for 30 min. The PCR product was analyzed by electrophoresis on 2,5% agarose gel in 1X Tris-Borate-EDTA buffer, then it was gel-purified with Wizard SV Gel and PCR Clean-Up System (Promega, Madison, Wisconsin, United States) and its concentration was determined by a spectrophotometer at 260 nm.
For the generation of *repertoires* of CDRs with different mutation rates, the pool of mutated CDR3s from this first mutagenesis step was sequentially re-

amplified, analyzed and purified 9 more times in the same conditions as described before; DpnI digestion was not performed after these amplification steps. In each amplification step, 10 pg of purified PCR product from the previous mutagenesis reaction were used as template and each PCR reaction was performed in triplicate to obtain enough DNA for the subsequent steps.

3.13. Topo cloning

To estimate the correlation between the mutation rate and the amount of template DNA, before sequence analysis, the CDR3s amplified from 1 ng, 100 pg and 10 pg of pYD1-D25-Aga2-HA plasmid were cloned by Zero Blunt® TOPO® PCR Cloning Kit (Invitrogen). Briefly, 2 µl PCR reaction were mixed to 1 µl salt solution, 1 µl vector and water, all supplied by the kit, in a final volume of 6 µl. The reaction was incubated at 25°C for 30 min and then 2 µl were used to transform 50 µl *E. Coli* DH5α, as described before. DNA was extracted from 30 randomly chosen clones and the inserts were analyzed by the Sanger sequencing.

3.14. High-throughput sequencing analysis of the repertoires of mutated CDR3s

The ten different repertoires of randomly mutated CDR3s were analyzed by high-throughput sequencing with a MiSeq apparatus (Illumina, San Diego, California, United States). The preparation of bar-coded fragments, sequencing reactions and data analysis were performed at the Center for Translational Genomics and BioInformatics, Hospital San Raffaele, Milan, Italy. TruSeq ChIP sample prep kit (Illumina) was used for the preparation of bar-coded fragments, then samples were diluted to a final concentration of 10 pM and sequenced in two runs, using 2x75 bp kit v3.

3.15. Generation of full length mutated scFvs

The scFv regions not involved in the mutagenesis were amplified from the plasmid pYD1-D25-Aga2-HA using the high fidelity Accuprime pfx DNA polymerase (Invitrogen) and then joined to the repertoire of mutated CDR3s by assembly PCR. The sequence upstream the CDR3 included all the VH of the scFv, except for the CDR3 and framework region 4; instead, the downstream sequence included the whole VL and framework region 4 of the VH. These sequences were amplified in two separate reactions, using 10 ng

of pYD1-D25-Aga2-HA plasmid as template, with the following primers and reaction conditions:
primers for upstream sequence
forward 5'-TGAAGAGGAAAAATTGGCAGTAACC -3' (primer 3 in fig. 10); reverse 5'-CTAGCACAGTAGTAAACAGCAGTATCTTC -3' (primer 4 in fig. 10);
primers for downstream sequence
forward 5'-TGGGGTCAAGGTACTATGGTTACTG -3' (primer 5 in fig. 10); reverse 5'-ATAAAGTATGTGTAAAGTTGGTAACGGAACG -3' (primer 6 in fig. 10);
amplification protocol: 15 sec denaturing at 95°C, 30 sec annealing at 58°C (upstream sequence) or 60°C (downstream sequence), 1 min extension at 68°C, 30 cycles of amplification.
Primers 4 and 5 were perfectly overlapping to primers 1 and 2, respectively (fig. 10), so that the amplified fragments had complementary ends with the CDR3, in order to allow their annealing during the assembly PCR reaction. Primers 3 and 6 were complementary to pYD1-D25-Aga2-HA plasmid; in this way, the assembled scFvs had 120 bp-homology ends with the linearized plasmid pYD1-D25-Aga2-HA, which promoted their *in vivo* recombination.
After treatment with DpnI to digest residual template DNA, the fragments were analyzed by electrophoresis on 1% agarose gel in 1X Tris-Acetate-EDTA buffer and gel-purified. For assembly PCR, 10 ng of each fragment were mixed to 10 ng of the pool of mutated CDR3s chosen for library generation; the reaction was performed with the following amplification protocol: 15 sec denaturing at 95°C, 30 sec annealing at 58°C, 1 min 40 sec extension at 68°C, 30 cycles of amplification.
Primers 3 and 6 indicated above were used for the assembly reaction. They were added to the reaction mixture during the denaturing step of the 6^{th} cycle, after fragments had annealed to each other and had been extended to produce full lenght scFv templates.
To check the contamination from the pYD1-D25-Aga2-HA plasmid in each of the three fragment preparations, as negative control, three separate assembly reactions were performed using only one of the three fragments as a template.

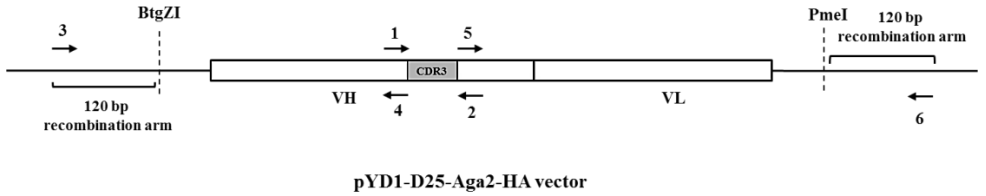

Fig. 10: design of the primers used for the amplification of the CDR3 flanking regions. The various couples of primers are described in the text. Primers 3 and 6 were also used for the assembly of these fragments with the mutated CDR3s. These oligoes were 120 bp far from BtgZI and PmeI restriction sites, respectively, which were used for pYD1-D25-Aga2-HA linearization. Therefore, the ends of the assembled scFvs had a sufficient length for recombination with the linearized plasmid.

3.16. Flow cytometry binding assays

Yeast cultures were induced overnight for 18h at 21°C at 0,5 OD/ml, in a shaking incubator at 200-250 rpm. 1x10^6 induced yeast cells were washed once with 1 ml Phosphate Buffered Saline 1X (PBS, Sigma) with 0,5% (w/v) albumine from bovine serum (BSA, Sigma), in a round-bottom 96 well plate, in a final volume of 200 µl, and centrifuged at 2000xg for 3 min at room temperature. Cells were incubated with different concentrations (from 10 pM to 30 nM) of human recombinant PD-L1 Fc-tagged (R&D Systems, Minneapolis, Minnesota, USA), diluted in 100 µl washing buffer, for 30 min at room temperature on a platform shaker with gentle agitation. A sample incubated with buffer only was used as blank. After binding of PD-L1, cells were incubated for 5 min on ice and then washed once as before. This step and the following ones were performed at 4°C to prevent dissociation of PD-L1 from scFv-displaying yeasts. For labelling of yeast-protein complexes, 1 µl of Alexa Fluor 488-conjugated anti-HA antibody (Biolegend, San Diego, California, USA) and 1:2000 APC-conjugated anti-human IgG, Fcγ specific antibody (Jackson immunoresearch, West Grove, Pennsylvania, USA) were used in 100 µl washing buffer. After 30 min incubation in agitation in the dark, cells were washed twice, resuspended in 200 µl PBS 1X and fluorescence was detected by CytoFLEX flow cytometer (Beckman Coulter, Brea, California, United States) and data analysis was performed by CytExpert software (Beckman Coulter). An unstained sample was used to fix fluorescence cut-off.

3.17. Cell sorting

The scFv-displaying yeasts that bound the antigen with high affinity were selected and isolated from the libraries by fluorescence activated cell sorting (FACS). For the first round of selection, a ten-fold excess of the library diversity was induced as above and $1x10^{\wedge 8}$ total induced yeast cells, split in 10 different aliquots of $1x10^{\wedge 7}$ cells each, were incubated with 30 or 10 nM human recombinant PD-L1 (see results) as before, in 200 µl washing buffer in 2 ml tubes. After 1x washing with 1 ml PBS 1X 0,5% BSA, the two fluorescent antibodies were added with the same concentrations indicated above, in a final volume of 200 µl washing buffer and incubated for 30 min in the dark. Cells were then washed twice and the pellet was kept on ice in the dark until sorting. Just before sorting, each aliquot of labelled cells was resuspended in 1,5 ml PBS 1X 0,5% BSA; sorting was performed with FACSaria IIIu (BD Biosciences, Franklin Lakes, New Jersey, United States) with the flow rate of 5000 evts/sec and data analysis was performed by FACSDiva 6.1.3 software (BD Biosciences). Sorted cells were recovered in 3-4 ml of selective medium, grown for 24h until saturation and then induced at a ten-fold excess of their diversity for the next selection.
For the subsequent rounds of selection, $1x10^{\wedge 7}$ total cells were stained. For library 3, two more sortings were performed, the second using 30 nM of PD-L1 and the third with 10 pM PD-L1. For library 10, one more sorting was performed at 10 nM. Cells were resuspended in 3 ml PBS 1X 0,5% BSA, sorted with a lower flow rate (1500 evts/sec) and recovered as described before.
For sortings, a diagonal gate was chosen which should include the APC-brightest yeast-PD-L1 complexes among the double-positive cells (see fig. 3, 7 and 8).

3.18. Estimation of diversity of sorted yeast populations

To evaluate the diversity of sorted populations, a sequencing analysis was performed by Sanger method on a small number of yeast clones. The plasmid DNA extracted from yeast is not suitable for sequencing, due to a high contamination from polysaccharides of yeast cell wall; for this reason, DNA extracted from fresh overnight yeast cultures was firstly transformed into *E. coli* DH5α, then 24 bacterial colonies were picked randomly, plasmid DNA was extracted and the CDR3s were sequenced with the forward primer 5'-CTCCAGGTAAAGGTTTGGAATGGG-3'.

3.19. mAb production

EBNA 293 cells were grown in 150 mm tissue culture dishes until they reached 70-80% confluency. They were co-transfected with 15 µg of plasmid pEU8.2 and 15 µg of plasmid pEU4.2 (see plasmids), encoding the heavy and light chain of each antibody (wild type or mutated D25 antibodies) respectively. Lipofectamine reagent 2000 (Invitrogen) was used for transfection according to the manufacturer's protocol. 6h post transfection, the culture medium was replaced by serum free medium CD CHO (Gibco), supplemented with 2mM L-glutamine (Gibco), 100U/ml penicillin and 100 µg/ml streptomicin (Gibco), 250 µg/ml Geneticin (G418 sulphate, Gibco), 2,5 µg/ml Amphotericin B (Gibco). After 5-6 days, media containing the secreted antibodies were collected and clarified at 2000 rpm for 30' at 4°C.

3.20. mAb purification

The mutated and the wild type anti-PD-L1 mAbs produced in EBNA cells were purified from the culture medium by protein A affinity chromatography, using Protein A HP Spin Trap (GE Healthcare, Chicago, Illinois, USA). Protein A resin was removed from the column and added to the culture medium (about 20 ml) collected from each transfected dish. Media were incubated with the resin for 3h at room temperature with low rotation and then centrifuged at 100xg for 30 sec; the medium was discarded and the resin, bound to the mAb, was resuspended in 600 µl of binding buffer (GE Healthcare) and re-loaded onto the column, previously equilibrated as indicated by the supplier. After centrifugation as before and two washes with 600 µl of binding buffer, mAbs were eluted from the resin with 400 µl of elution buffer (GE Healthcare) by centrifugation and collected in a sterile 2 ml tube containing 30 µl of neutralization buffer (GE Healthcare). This step was repeated once again in a different tube, in order to collect a second elution fraction.

3.21. Protein quantification and coomassie staining

The antibody concentration in the eluted fractions was determined using Pierce BCA Protein Assay Kit (Thermo Fisher Scientific). In brief, 2 µl of purified antibody were mixed with BCA reagent according to manufacturer's recommendations, then samples were heated at 60°C for 30 min and

absorbance was read with a spectrophotometer (562 nm). The concentrations were estimated using a standard curve of BSA, supplied by the kit.
The molecular weight of the antibodies and the purity of the preparations were checked by sodium dodecyl sulfate polyacrylamide gel electrophoresis (SDS-PAGE), followed by coomassie staining. For reducing SDS-PAGE, 3 µg of purified antibody were mixed to 10% (v/v) β-mercaptoethanol, boiled at 95°C for 10 min and then loaded on a 4-12% denaturing gel (Invitrogen) with 4x loading dye Sample Buffer (Invitrogen). For not reducing SDS-PAGE, 1 µg of each antibody was loaded onto the gel. Proteins were then fixed on the gel and stained with Coomassie Brilliant Blue R-250 Staining Solution (Biorad) for 30 min at room temperature with gentle shaking. The excess of dye was removed by using 30% ethanol and 10% acetic acid in distilled water, until protein bands were visible.

3.22. Flow cytometry binding assays of mAbs to hPBMCs

hPBMCs were thawed in RPMI 1640 medium, supplemented with 2mM L-glutamine, 1% (v/v) of CTL wash supplement (CTL, Shaker Heights, Ohio, USA) and 100U/ml Benzonase (Merck Millipore, Burlington, Massachusetts, United States) and centrifuged at 1200 rpm for 10 min. they were then resuspended in complete RPMI medium (see “cell lines and culture media”) and plated at about 8-106 cells/well in a 12 well plate. After resting for 16h, hPBMCs were counted, re-suspended at 106 viable cells/ml in complete medium and activated with Dynabeads Human T-Activator CD3/CD28 (Gibco), 25 µl beads/106 viable cells, in a 12 well plate. 24h post activation, the not activated and activated cells were centrifuged and plated at 4x105 cells/well in 100 µl PBS in a 96 well plate with round bottom. After one wash in PBS, they were incubated with 50 µl LIVE/DEAD™ Fixable Violet Dead Cell Stain (Invitrogen) for 30 min at +4°C and washed once again. The mAbs, diluted in 100 µl PBS at concentrations ranging from 6 nM to 9,6 pM, and the anti-human PD-L1 antibody (G&P Biosciences, Santa Clara, California, USA) diluted 1:1000 were added to the cells and incubated for 1h 30 min at room temperature in the dark with gentle shaking. The cells were washed twice with 200 µl PBS and incubated with 5 µl of PE-conjugated anti-human CD2 (BD Biosciences) and 1:2000 APC-conjugated anti-human IgG, Fcγ specific antibody (Jackson immunoresearch), diluted in 100 µl PBS1X 1% (v/v) FBS (FACS buffer). After 45 min incubation as before, two washes with FACS buffer were performed and cells were then resuspended in

150 µl PBS1X for the acquisition at CytoFLEX flow cytometer (Beckman Coulter).

4. RESULTS

4.1. Multi-step and CDR-targeted random mutagenesis of an anti PD-L1 scFv

A single chain variable fragment (scFv) specific for PD-L1 protein and named D25 was previously identified from a phagemid library by our side (unpublished data). To improve affinity of this antibody fragment for its target, *repertoires* of mutants were generated by random mutagenesis and the variants were selected by a yeast display platform.
Since it has been demonstrated that engineering the variable regions can have effects on many features of an antibody, other than its binding properties (Tomoyuki et al, 2011), mutagenesis was restricted only to the sequences of the antigen binding site (CDRs), keeping the framework sequences unaltered. As result, a CDR-targeted mutagenesis approach was used and restricted to the CDR3 (33bp in length) of the VH (fig. 11).

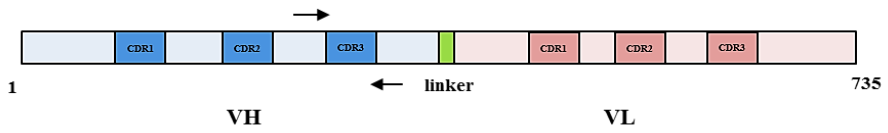

Fig. 11: scheme of D25 scFv (735 bp). Heavy and light chain variable regions (VH and VL) and their CDRs are represented in blue and pink respectively. Black arrows indicate the primers used for the CDR3 (33 bp) mutagenesis.

In an attempt to obtain a *repertoire* of fragments containing the maximum possible diversity of mutants and a very low abundance of the starting wild type sequence, the CDR3 of D25 was amplified by an error-prone polymerase for random insertion of point mutations.
As the mutation frequency is inversely correlated with the number of molecules used as template for the amplification, a preliminary step of mutagenesis was performed to determine the right amount of template DNA. The wild type CDR3 sequence was amplified using different amounts of template plasmid pYD1-D25-Aga2-HA, i.e. 1 ng, 100 pg, 10 pg and 1 pg. In

all these amplification reactions, the number of PCR cycles, which also influences the mutation frequency, remained constant.
The CDR3 amplification was confirmed by the presence of the expected molecular weight band (88 bp), except for the reaction obtained from 1 pg of template, in which no PCR product was observed (fig. 12).

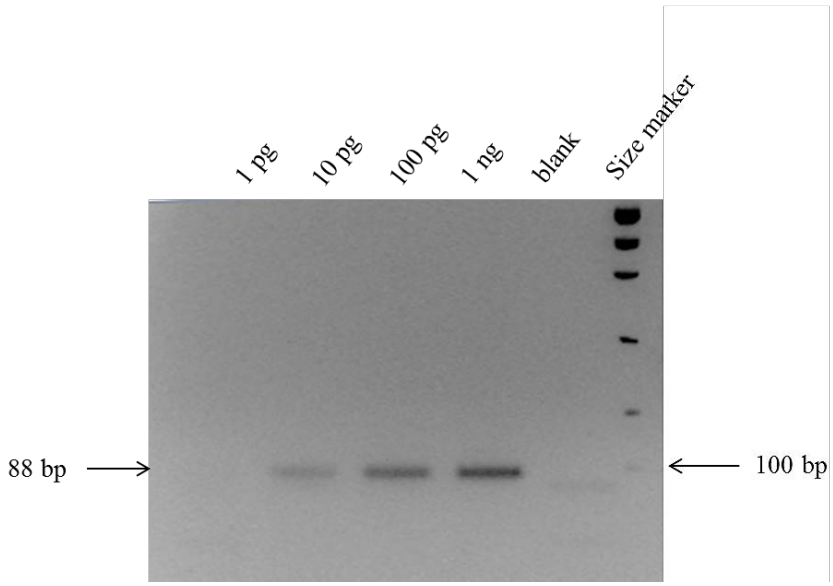

Fig. 12: electrophoretic analysis of the error-prone PCR products obtained from different amounts of wild type scFv D25. At the top of each lane the amount of template DNA used in the CDR3 amplification reaction is indicated. The entire volume of each PCR reaction was loaded on the gel.

To have an idea of the mutation rate obtained in these amplification conditions, the three purified PCR products were cloned by a topo-cloning system and the sequence of 30 randomly chosen clones was analyzed by the Sanger method. Sequencing analysis revealed that only 23-26% of the CDR3s carried point mutations. As no significant difference was observed among the three amplification conditions and considering that 1 pg of template didn't result in an efficient amplification, 10 pg was considered the minimum amount of template for the mutagenesis.
To increase the mutation frequency, an approach based on multiple mutagenesis rounds was chosen: the pool of CDR3s from the first mutagenesis step was purified and re-amplified 9 times using the same PCR conditions (see materials and methods). After that, a systematic analysis was

carried out by high-throughput sequencing on the pools of CDR3s obtained at each step of mutagenesis (1 to 10).

4.2. High-throughput sequencing of the different repertoires of mutants

Fragments from the 10 mutagenic PCR reactions were bar-coded and then sequenced in two runs on a MiSeq apparatus. To be sure of the correct sequence of each fragment, both forward and reverse strand of each molecule were sequenced and the number of reads obtained (i.e. the number of sequenced molecules) was in the same order of magnitude for all samples (between $5x10^5$ and $2{,}2x10^6$).
Several parameters were evaluated by bioinformatics analysis.The frequency of wild type CDR3 nucleotide sequences showed an inverse correlation with the number of mutagenesis rounds (fig. 13). In particular, a 50% reduction of wild type was obtained if only one round of mutagenesis was performed, while a 95% decrease was observed after 10 rounds. The reduction of wild type followed a non-linear trend and the magnitude of this decrease became progressively lower; after a fast drop at round 1, about a 10% reduction occurred at steps 2 and 3, while it was about 5% at each step between 4 and 7 and 3% at each of the last three rounds.

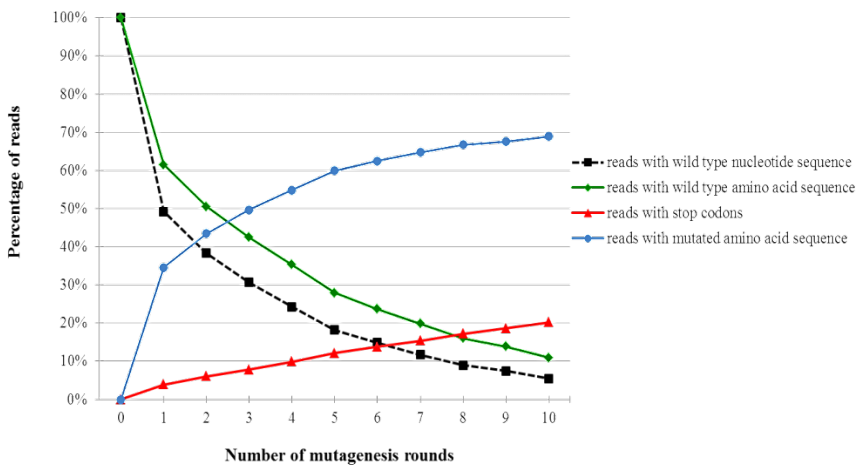

Fig. 13: high-throughput sequencing analysis performed on the pools of CDR3s amplified at each round of mutagenesis. The decrease, as percentage, of reads showing wild type CDR3 nucleotide sequence is

indicated as dotted black line (squares). The resultant translated sequences are plotted as percentage of wild type (green line - romboids), stop codon (red line - triangles) and missense mutants (blue line - circles).

The same analysis was carried out after translating all reads into their corresponding amino acid sequence. As shown in fig. 13, the reduction trend of the translated wild type CDR3 was the same as that one observed for the nucleotide sequences, but because of the presence of sequences containing silent mutations, in each round more translated wild type CDR3s than nucleotide ones were found. The difference between amino acid and nucleotide wild type sequences was about 12% at round 1, while slowly decreased to 5% at round 10.

The fraction of reads containing stop codons was also evaluated as a measure of the number of truncated scFvs that were likely to be lost during selection because not expressed or unable to bind the antigen. As expected, the higher the number of point mutations accumulated in the sequences, the higher the chance to introduce stop codon triplets too. In fact, these sequences represented only 4% of the entire *repertoire* at round 1, but rose to 20% at round 10. As opposed to wild type sequences, the change in number of reads with stop codons showed a linear trend (red line in fig. 13), with a constant increase of about 2% at each mutagenesis step.

The remaining fraction of reads of each round was represented by sequences carrying missense mutations (shown in blue line, fig. 13). The first round alone was able to increase their percentage up to 35%, while from round 2 these mutated sequences increased very slowly, until they reached a peak of 70% at round 10.

To evaluate the diversity of the reads carrying missense mutations, the percentage of different nucleotide sequences found in this group was determined for each mutagenesis round. As reported in table 2, a three-fold increase in diversity was reached at round 10 compared to round 1.

mutagenesis round	reads showing different sequences (% of reads containing missense mutations)	fold change compared to round 1
1	6,2%	1,0
2	6,6%	1,1
3	9,8%	1,6
4	9,9%	1,7
5	13,2%	2,2
6	11,9%	2,0
7	12,2%	2,0
8	16,1%	2,7
9	16,0%	2,7
10	18,0%	3,0

Table 2: diversity of non-stop mutated sequences. The level of diversity of sequences containing missense mutations was evaluated as percentage of reads showing a different sequence. The increase in diversity is expressed as fold change compared to round 1.

In addition, the abundance of single, double, triple, or more mutations was evaluated in the sequences of each mutagenesis round. The trend of the mutation number in the translated reads is shown in fig. 14.
Reads containing 1 mutation were the most abundant mutated sequences in almost all rounds (except for round 10); they represented more than half of the mutated reads at round 1 (57%) and decreased up to round 10, where their fraction was about two-fold lower than the first round.
Reads with 2 mutations were four-fold lower than those with 1 mutation at round 1 (about 15% of the mutated reads) and progressively increased during mutagenesis. At round 7 they reached a plateau until round 10, where their fraction was the same as sequences containing 1 mutation.
Sequences carrying 3 mutations increased too and showed a linear trend from round 2 to the end of the mutagenesis. The percentage of sequences with 4 mutations, instead, was constant from round 1 to 6 (about 3% of the mutated sequences) and slightly increased only in the last rounds (6% at round 10).

Sequences that accumulated 5 or more mutations (5 to 25) were less frequent; in fact, each of these subgroups corresponded to a variable, but low fraction of the total reads (from 0,1% to 3%), depending on the mutagenesis round. However, if considered all together, they ranged from 18% of mutated reads at round 1 to 27% at round 10 (light blue bar in fig. 14).
Up to 31 mutations were found in the same sequence, but these cases were indeed very rare. In fact, the reads containing a number of mutations between 26 and 31 represented only 0,001-0,006% of the mutated ones in some cycles.

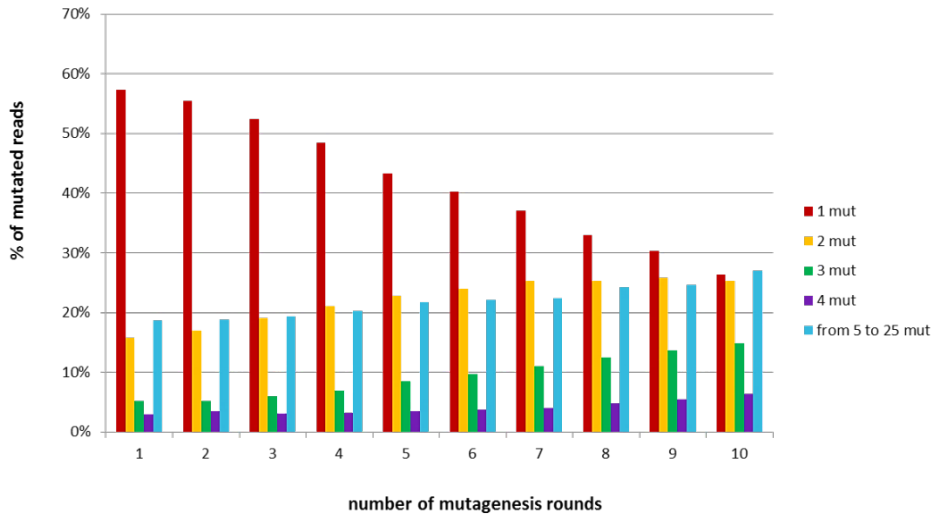

Fig. 14: distribution of single and multiple mutations in the 10 pools of translated CDR3s. The prevalence of each group is expressed as percentage of the mutated reads. Sequences with 1 to 4 substitutions were the most abundant and all of them, with the exception of reads with 1 mutation (red bar), showed an increasing trend. In the last bar (light blue) all sequences carrying from 5 to 25 mutations are grouped.

4.3. Generation of CDR3-mutated D25 yeast libraries

To select the scFv D25 mutants with improved affinity for PD-L1, a yeast display platform was used. This system is based on the expression of the antibody fragments on *S. Cerevisiae* surface (as fusion proteins with the cell

wall a-agglutinin Aga) and the subsequent screening of their binding properties to the target antigen.
Considering the overall distribution of mutations introduced in the 10 rounds of mutagenesis, the CDR3 fragments from cycles 3 and 10 were chosen to generate the yeast libraries. In round 3 the percentage of mutated sequences started to exceed that of the wild type (fig. 13) and the majority of them harbored single point mutations (fig. 14); on the other hand, round 10 corresponded to the condition in which the fraction of wild type sequences was the lowest of all rounds (fig. 13). In addition, sequences carrying single and double mutations were present at the same level and there was also a significant increase in the fraction of different clones containing missense mutations compared with round 1 (table 2).
To generate each library, the scFv regions not involved in the mutagenesis were amplified by a high-fidelity polymerase from the wild type sequence and, thanks to overlapping ends (see materials and methods), they were joined to the pool of the mutated CDR3s by assembly PCR (fig. 15, panel A). This reaction produced a pool of full-length scFvs whose sequences differed only in their CDR3. They were subsequently cloned by *in vivo* recombination into the yeast expression plasmid pYD1-D25-Aga2-HA, previously linearized and depleted of the wild type scFv. The recombination was allowed by two homology arms added to 5' and 3' of the scFvs in the high-fidelity amplification step (fig. 15, panel B).
The *in vivo* recombination efficiency was estimated by plating serial dilutions of the libraries and counting the colony forming units. Considering that the maximal theoretical diversity achievable in yeast libraries is 10^9, high and comparable titers were obtained for both libraries: around $2x10^8$ scFv clones from the CDR3s mutated at cycle 3 (hereafter library 3) and approximately $1,7x10^8$ scFv clones from the CDR3s mutated at cycle 10 (hereafter library 10).

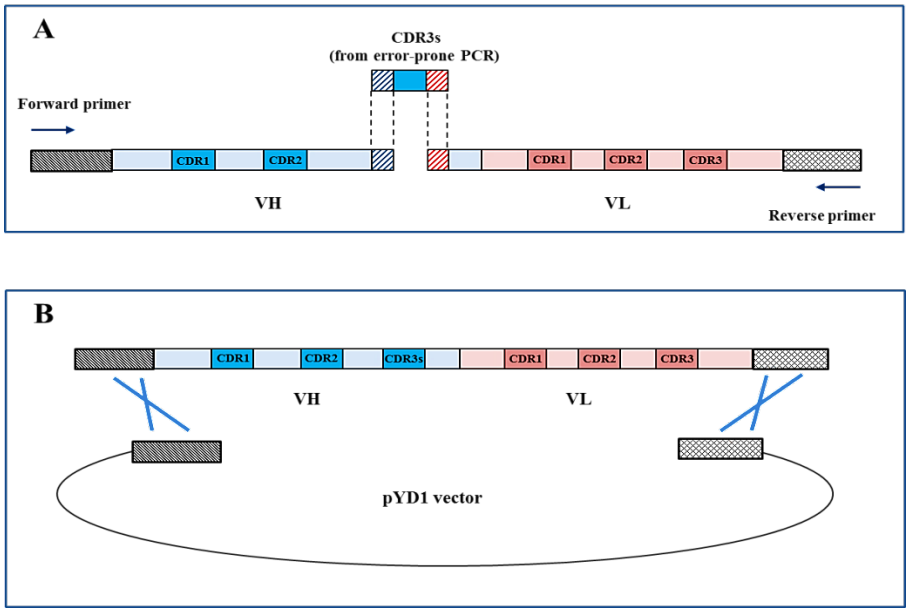

Fig. 15: production of full-lenght scFvs by assembly PCR and *in vivo* recombination. The CDR3s obtained from mutagenesis were joined to the flanking regions of the wild type scFv thanks to their little overlapping sequences (blue and red-striped boxes in panel A). The annealed fragments were then amplified with two of the primers used for VH and VL high-fidelity amplification. The scFvs contained homology ends with the expression plasmid pYD1, in order to allow insertion by *in vivo* homologous recombination (panel B).

4.4. Set up of flow cytometry analyses for library selection

Before starting library selections, the experimental conditions for the flow cytometry assays were set up on the wild type yeast. To obtain this clone, the parental yeast strain was transformed with the plasmid pYD1-D25-Aga2-HA, encoding for the fusion protein between the wild type D25 scFv and Aga2p subunit of a-agglutinin, with the HA tag at the C-terminus. This cassette was *de novo* synthesized (see materials and methods) with an optimized codon usage for expression in yeast, in order to provide the highest possible production and display of the scFv.
The two fluorescent antibodies used for the detection of the yeast-scfv-PD-L1 complex, the Alexa Fluor 488-conjugated anti-HA antibody (AF488-HA) and the APC-conjugated anti-Fc antibody (APC-Fc), were initially tested, alone

and in combination, on induced and not induced wild type yeast without the antigen. As shown in fig. 16A, AF488-HA specifically recognized only the induced yeast that displayed the HA-tagged scFv; on the contrary, the APC-Fc antibody used for the recognition of the Fc-tagged PD-L1 antigen (PD-L1 Fc), didn't bind either to induced or not induced yeast. The same result was obtained if these antibodies were used in combination. On the other hand, only in presence of PD-L1 Fc, an APC positive population appeared in the induced yeast (fig. 16B). These results demonstrated that the wild type scFv D25 was fully expressed on yeast surface and was able to bind to PD-L1 antigen.

In this set up phase, the most appropriate PD-L1 concentrations to be used for selection were also determined. For this reason, a binding curve of the wild type yeast-scFv was made to PD-L1 concentrations ranging from 10 pM to 30 nM. Yeast cells, stained with the two antibodies as before, were analyzed by flow cytometry and APC mean fluorescence intensity (MFI) of PD-L1 binding population (blue cells in fig. 16B) was plotted as a function of PD-L1 concentration. Using 10 pM of target antigen, almost no binding was detected, while from 10 nM ongoing all binding sites on the wild type yeast surface were saturated.

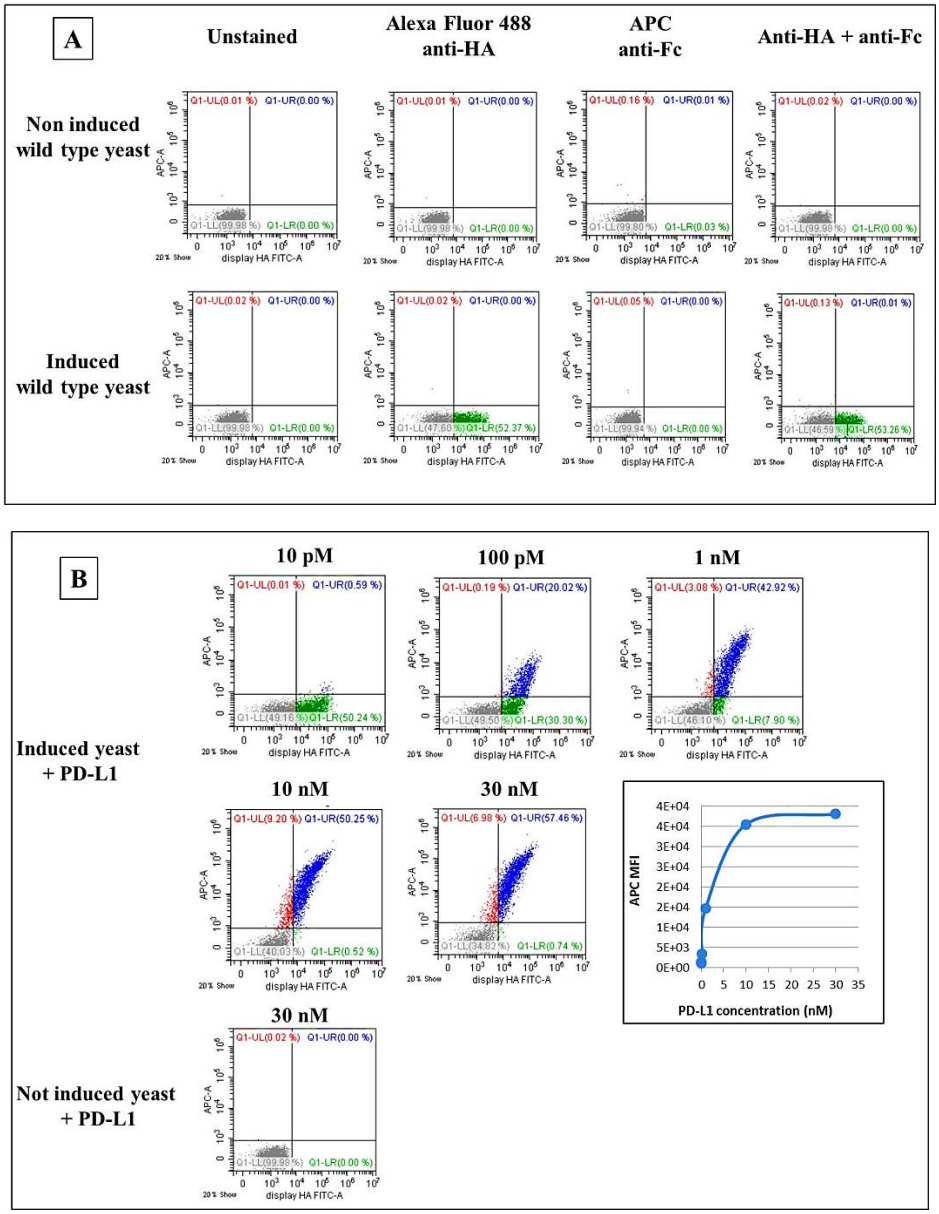

Fig. 16: set up of flow cytometry assays. Panel A: the antibodies for the flow cytometry analyses were tested on induced and not induced yeast, in absence of the antigen. No fluorescence was detected in not induced yeast (upper plots), whereas a specific signal of the anti-HA antibody was only detected in induced yeast (lower plots). Panel B: a binding curve of the wild type yeast-scFv D25 to PD-L1 was performed; the saturation concentration of antigen didn't bind to the not induced yeast (last plot).

4.5. Cell sorting-based selection of high affinity anti-PD-L1 scFvs from the library 3

For isolation of high affinity scFvs from the library 3, three rounds of selection were performed and the selection stringency was progressively increased at each step by reduction of PD-L1 concentrations and/or by a more selective sorting gate.
In order to keep a good representation of the mutants from library 3 and to avoid that antigen concentration would be limiting, in the first round of selection $1x10^8$ yeast cells were incubated with a saturation concentration of PD-L1 (30 nM).
The yeast-scFvs-PD-L1 complexes were labelled and analyzed by flow cytometry; in order to exclude from the sorting gate the non-specific signal due to the anti-PD-L1 Fc antibody, control samples without antigen were included in all sortings (fig. 17, middle column).
As shown in fig. 17 (round 1 row), more than half of the yeasts (56,9%) expressed a scFv on their surface (Alexa-488 positive cells) with various degrees of display and 65% of these scFv-displaying cells were also able to bind to PD-L1. A diagonal sorting gate was defined which included about 9% of these PD-L1 binding cells; in this way, for each display level, the APC-brightest yeast-PD-L1 complexes were sorted. The cells included in the sorting gate were recovered (about $3x10^5$ total cells at the end of the sorting), amplified and induced again for the following selection step.
For the second selection round, $1x10^7$ cells from the previous step were incubated with the same PD-L1 concentration as before and then stained. The flow cytometry analysis (round 2 row in fig. 17) showed that this population displayed the scFvs at a comparable level to the parental library (61,3%), but a higher percentage of these scFv-displaying cells (78%) bound to PD-L1. At this step a more stringent sorting gate was used, including only 1,1% of the PD-L1 binding cells. The $2x10^4$ sorted yeasts were amplified and, before going on with additional rounds, some of them (24 clones) were checked by Sanger sequencing. The analysis of the amino acid sequence revealed that only 17,4 % of the sorted clones carried a mutation in the CDR3 (data not shown). Considering that the fraction of mutated CDR3s in the DNA coming from mutagenesis cycle 3 (used to generate this library) was 50% (fig. 13), a great loss of mutants occurred during these selection steps.
In attempt to counter-select the wild type yeasts still present at a high percentage in this population, a third and final selection round was performed using 10 pM PD-L1 antigen, because the wild type yeast showed a very low binding level at this concentration (fig. 16B). In this very stringent condition only 0,05% of the displaying cells from sorting 2 was able to bind the antigen (fig. 17, round 3 row) and, although not clearly visible, the sorting gate

included 17,6% of these antigen binding yeasts. With this strategy only a total of 75 yeasts were sorted from $1x10^7$ initial stained cells.

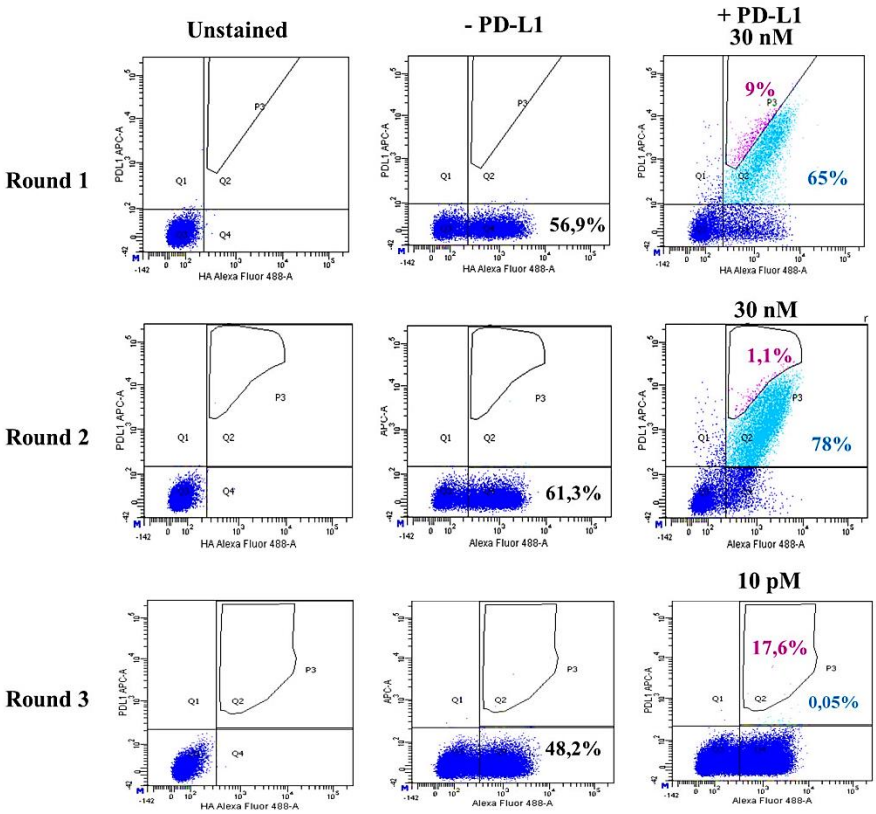

Fig. 17: sorting strategy for the selection of high affinity scFvs from the library 3. Unstained samples showed in left column were used to determine fluorescence thresholds. Control samples shown in the middle column were stained with both the antibodies and without the target antigen, in order to leave any non-specific signal out of the sorting gate. Percentages shown in middle plots (lower right quadrants) indicate scFv-displaying yeasts; in the right plots, blue percentages (upper right quadrants) correspond to the fraction of displaying cells also binding to PD-L1, while in purple (poligonal P3 gate) percentages of sorted cells are shown and expressed as fraction of PD-L1 binding cells.

4.6. Cell sorting-based selection of high affinity anti-PD-L1 scFvs from library 10

The selection of mutated D25 scFvs from the library 10 was made by a different sorting scheme. In order to quicken the overall procedure, only two sorting rounds were performed and a higher selection stringency was used.
In the first step, $1x10^8$ cells from the library were induced as usual, incubated with a saturation concentration of the target antigen (10 nM, fig. 16B) and then stained for a flow cytometry analysis. In this library, 33% of the cells expressed the scFvs and about 39% of them bound to the antigen (fig. 18, round 1 row). Then, in order to avoid the carry-over of the wild type yeast since the beginning of the selection, the sorting gate was restricted to only the 1,2% of the PD-L1 binding cells (fig. 18, right column). The $5x10^4$ recovered yeasts were amplified and induced for the subsequent selection step.
The second and last round was performed in the same conditions as for round 3 of library 3 (fig. 17); $1x10^7$ cells derived from the amplification of the yeasts sorted at round 1 were incubated with 10 pM PD-L1, stained and analyzed by flow cytometry. As shown in fig. 18, round 2 row, 55,3% of the yeasts displayed the scFvs and 0,4% of them were able to bind to this low antigen concentration. The sorting gate chosen for this selection included 0,2% of the scFv-PD-L1 complexes with the brightest APC fluorescence and led to the recovery of about 900 yeast cells. In the absence of PD-L1 antigen, no double AF488/APC signal was observed either in round 1 or in round 2 (fig. 18, middle panels).

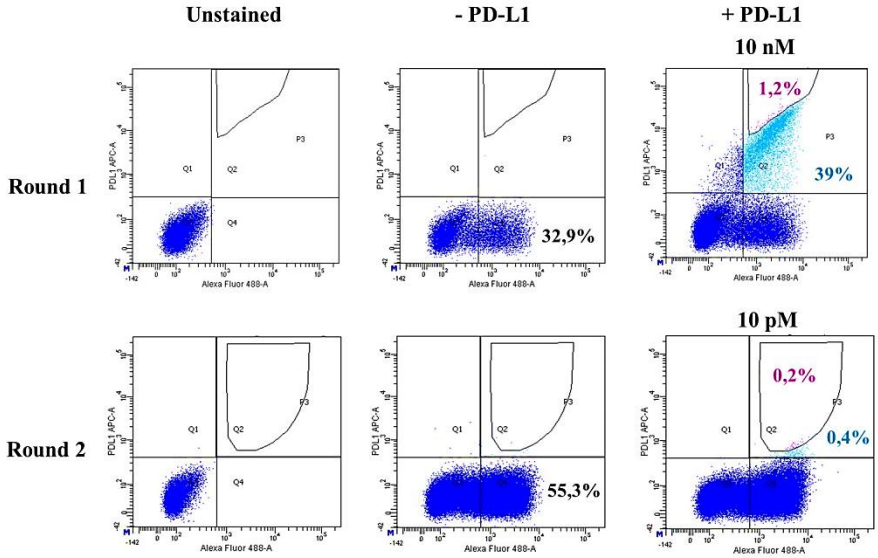

Fig. 18: sorting strategy for the selection of high affinity scFvs from library 10. Percentages in black refer to the scFv-displaying yeasts (lower right quadrants in middle plots), while those in blue (upper right quadrants in left plots) indicate which fraction of them bound to PD-L1. Percentages in purple correspond to the fraction of binding cells that were selected for sorting. In the left and middle columns, control unstained yeasts and stained yeasts without target antigen are shown, respectively.

4.7. Flow cytometry analysis of PD-L1 binding to the sorted populations from library 3 and library 10

To evaluate the effectiveness of the selections, the yeast populations sorted from each library were amplified and then tested for their binding properties to PD-L1 in comparison with the wild type yeast.
Cells were incubated with the same PD-L1concentration used for the last selection step (10 pM), stained as usual and then analyzed by flow cytometry. As shown in fig. 19, while only 1,2% of the cells displaying the wild type scFv bound to PD-L1, confirming the previous data (fig. 16B), in the yeast population sorted from library 3 31% of the scFv-displaying cells was able to bind the antigen; interestingly, for the yeast cells sorted from library 10 the result was even better, with almost half (45,5%) of the scFv-expressing yeasts that bound to PD-L1. The results were not influenced by the scFv display levels, as they were fairly high for all the three samples (from about

60% for the wild type to 74% for cells selected from library 10, second column, fig. 19).
These results suggested that the yeast populations selected from the two libraries contained yeast clones with an improved binding affinity to PD-L1 antigen compared with the wild type yeast.

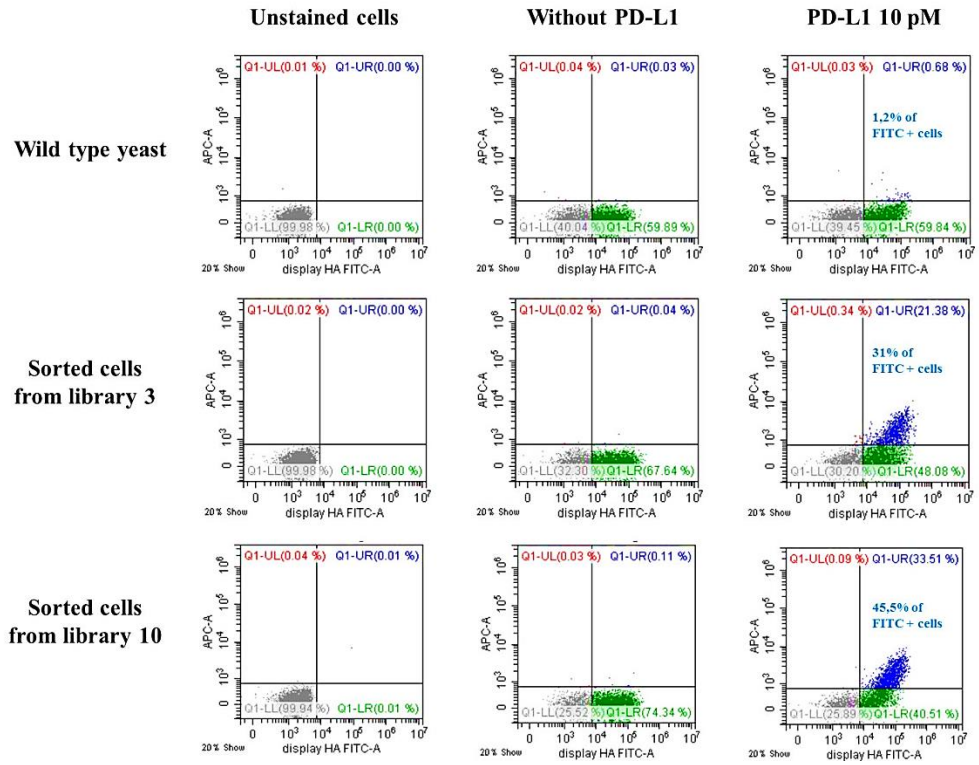

Fig. 19: binding assay of PD-L1 to the yeast populations selected from the libraries 3 and 10. The percentages of each subpopulation are indicated in each quadrant and expressed as fraction of total cells. Only PD-L1 binding cells (blue in right panels) are also expressed as percentage of scFv-displaying yeasts. These displaying cells represent more than half of total cells in both sorted populations and the wild type yeast (FITC + population in green in the middle panels). Unstained samples (left panels) were used to fix the fluorescence cut-off.

4.8. Sequencing of random clones from the yeast populations selected from library 3 and 10

To evaluate if both sortings led to a reduction of the wild type clones and an enrichment of the mutants ones, the plasmid DNA was extracted from the pool of yeast cells selected from each library and the scFvs were sequenced. As DNA directly extracted from yeasts can't be easily manipulated for downstream applications, including sequencing analysis, it was firstly transformed into bacterial cells and then extracted again from 24 randomly chosen colonies of each sorted library. The whole scFvs were sequenced by Sanger method and the amino acid sequences were analyzed in comparison with the wild type one.

Among the clones sequenced from sorted library 3, only 25% of them carried the wild type CDR3, while the remaining 75% were mutated (18 of 24 sequences) and contained single or double mutations (6 and 12 clones respectively) in the CDR3. Interestingly, mutations affected always the same positions, i.e. the first and the tenth CDR3 amino acid (table 3). In particular, in the first position a Thr to Ser substitution was always found, except for a single clone in which Thr was replaced by Ala. In the 12 sequences with two mutations, Ser was coupled with another substitution that always affected the tenth amino acid of the CDR3 (Asp to Asn substitution in 2 clones; Asp to Gly in 7 clones; Asp to Ala in 2 clones; Asp to Tyr in 1 clone). A single clone carrying only the Asp to Tyr substitution in the tenth position was also found.

These results showed that a high percentage of mutants was selected from library 3 and 7 out of 18 mutated clones carried different mutations (table 5).

About library 10 (table 4), no wild type clones were found among the 24 sequences analyzed, which carried one, two or three mutations (8,3%, 75% and 16,6% of the total clones, respectively). The mutations affected the first, the tenth and, less frequently, the ninth CDR3 amino acid positions. In the double mutants, which represented the majority of the clones, one of the two mutations always fell at the tenth position of the CDR3, where the Asp was replaced by a Gly or an Asn; the second mutation was at the first position (a Thr to Ser substitution) except for 3 clones, where it affected the ninth amino acid (a Tyr to Phe substitution).

Those mutants with the Ser + Gly and Ser + Asn substitutions were the most enriched ones (9 and 6 copies, respectively) and they were also found in library 3 (table 5).

In the triple mutant clones, the Ser + Gly mutations were coupled to the Tyr to Phe substitution in the ninth position or, only in a single clone, to a Tyr to Asn at the eleventh amino acid.

In the remaining clones, a single amino acid substitution was found at the ninth position, which corresponded to the same mutation found in some double or triple mutants.
In conclusion, 7 types of different clones were obtained from this small scale sequence analysis of sorted library 10, two of which were also found in library 3 (table 5).

	CDR3 amino acid position										
	1	2	3	4	5	6	7	8	9	10	11
wild type	**T**	**K**	**W**	**E**	**L**	**V**	**D**	**P**	**Y**	**D**	**Y**
clone 3_1	A	K	W	E	L	V	D	P	Y	D	Y
clone 3_2	S	K	W	E	L	V	D	P	Y	D	Y
clone 3_3	S	K	W	E	L	V	D	P	Y	N	Y
clone 3_4	T	K	W	E	L	V	D	P	Y	Y	Y
clone 3_5	S	K	W	E	L	V	D	P	Y	G	Y
clone 3_6	S	K	W	E	L	V	D	P	Y	D	Y
clone 3_7	S	K	W	E	L	V	D	P	Y	Y	Y
clone 3_8	S	K	W	E	L	V	D	P	Y	D	Y
clone 3_9	S	K	W	E	L	V	D	P	Y	G	Y
clone 3_10	S	K	W	E	L	V	D	P	Y	G	Y
clone 3_11	T	K	W	E	L	V	D	P	Y	D	Y
clone 3_12	T	K	W	E	L	V	D	P	Y	D	Y
clone 3_13	S	K	W	E	L	V	D	P	Y	G	Y
clone 3_14	S	K	W	E	L	V	D	P	Y	G	Y
clone 3_15	S	K	W	E	L	V	D	P	Y	N	Y
clone 3_16	T	K	W	E	L	V	D	P	Y	D	Y
clone 3_17	S	K	W	E	L	V	D	P	Y	A	Y
clone 3_18	S	K	W	E	L	V	D	P	Y	D	Y
clone 3_19	T	K	W	E	L	V	D	P	Y	D	Y
clone 3_20	S	K	W	E	L	V	D	P	Y	G	Y
clone 3_21	T	K	W	E	L	V	D	P	Y	D	Y
clone 3_22	T	K	W	E	L	V	D	P	Y	D	Y
clone 3_23	S	K	W	E	L	V	D	P	Y	A	Y
clone 3_24	S	K	W	E	L	V	D	P	Y	G	Y

Table 3: sequences of the VH CDR3s of randomly chosen clones selected from the library 3. The amino acid sequence of the wild type CDR3 (second raw, bold red) and the corresponding amino acid positions (raw above) are reported in the table. The other raws show the sequences of 24 randomly chosen yeast clones obtained from the selection of the library 3. In the yellow boxes the amino acid substitutions are indicated. The number of each clone is preceded by the number of the library.

	CDR3 amino acid position										
	1	2	3	4	5	6	7	8	9	10	11
wild type	T	K	W	E	L	V	D	P	Y	D	Y
clone 10_1	T	K	W	E	L	V	D	P	F	D	Y
clone 10_2	S	K	W	E	L	V	D	P	Y	G	Y
clone 10_3	S	K	W	E	L	V	D	P	F	G	Y
clone 10_4	S	K	W	E	L	V	D	P	Y	N	Y
clone 10_5	S	K	W	E	L	V	D	P	Y	N	Y
clone 10_6	S	K	W	E	L	V	D	P	Y	G	Y
clone 10_7	S	K	W	E	L	V	D	P	Y	G	Y
clone 10_8	T	K	W	E	L	V	D	P	F	N	Y
clone 10_9	S	K	W	E	L	V	D	P	Y	G	Y
clone 10_10	S	K	W	E	L	V	D	P	Y	G	Y
clone 10_11	S	K	W	E	L	V	D	P	Y	N	Y
clone 10_12	S	K	W	E	L	V	D	P	Y	G	N
clone 10_13	T	K	W	E	L	V	D	P	F	N	Y
clone 10_14	T	K	W	E	L	V	D	P	F	G	Y
clone 10_15	S	K	W	E	L	V	D	P	Y	N	Y
clone 10_16	S	K	W	E	L	V	D	P	Y	G	Y
clone 10_17	T	K	W	E	L	V	D	P	F	D	Y
clone 10_18	S	K	W	E	L	V	D	P	Y	N	Y
clone 10_19	S	K	W	E	L	V	D	P	Y	G	Y
clone 10_20	S	K	W	E	L	V	D	P	Y	G	Y
clone 10_21	S	K	W	E	L	V	D	P	Y	N	Y
clone 10_22	S	K	W	E	L	V	D	P	Y	G	Y
clone 10_23	S	K	W	E	L	V	D	P	F	G	Y
clone 10_24	S	K	W	E	L	V	D	P	F	G	Y

Table 4: sequences of the VH CDR3s of randomly chosen clones selected from library 10. The color code is the same as in table 3.

4.9. Generation of the individual mutated yeast clones and binding assay to PD-L1

To confirm that all the different mutated scFvs identified by sequencing analysis (table 5) really had an improved affinity for PD-L1 protein, the plasmid DNA encoding for each of these scFvs was transformed into the parental yeast strain, in order to obtain the individual yeast-scFv clones. After growing and induction, all these clones, along with the wild type yeast, were incubated with the same PD-L1 concentration used for the last sorting (10 pM), then stained and analyzed by flow cytometry. Clones isolated from library 3 and library 10 were tested in two independent experiments, along with the wild type yeast as control.
Among the seven different clones derived from the library 3 selection, 4 of them showed an improved binding compared with the wild type one (clones 3_3, 3_7, 3_14 and 3_17), as indicated by the percentages of the PD-L1 binding cells in fig. 20A (blue populations). These corresponded to the scFvs that carried the double substitutions. One clone (clone 3_1, with Thr to Ala substitution at the first CDR3 amino acid position, table 5) displayed its scFv

at a lower level than the previous ones and its binding to the target antigen was very low too, while the two other single mutant clones (number 3_2 and number 3_4 in table 5 and fig. 20A) didn't express their respective scFvs at all.

A similar result was obtained for the clones selected from library 10; in fact, except for 2 clones which didn't were able to display their scFv (clones 10_8 e 10_14 in fig. 20B and table 5), 4 out of the seven different clones bound to PD-L1 better than the wild type one, as demonstrated by the presence of the double positive population in their corresponding dot plots (clones 10_2, 10_3, 10_4 and 10_12 in table 5). In particular, two of these clones (10_2 and 10_4) were shared with library 3. Only one clone (clone 10_1 in fig. 20B) bound to this antigen concentration very weakly, despite its good display level.

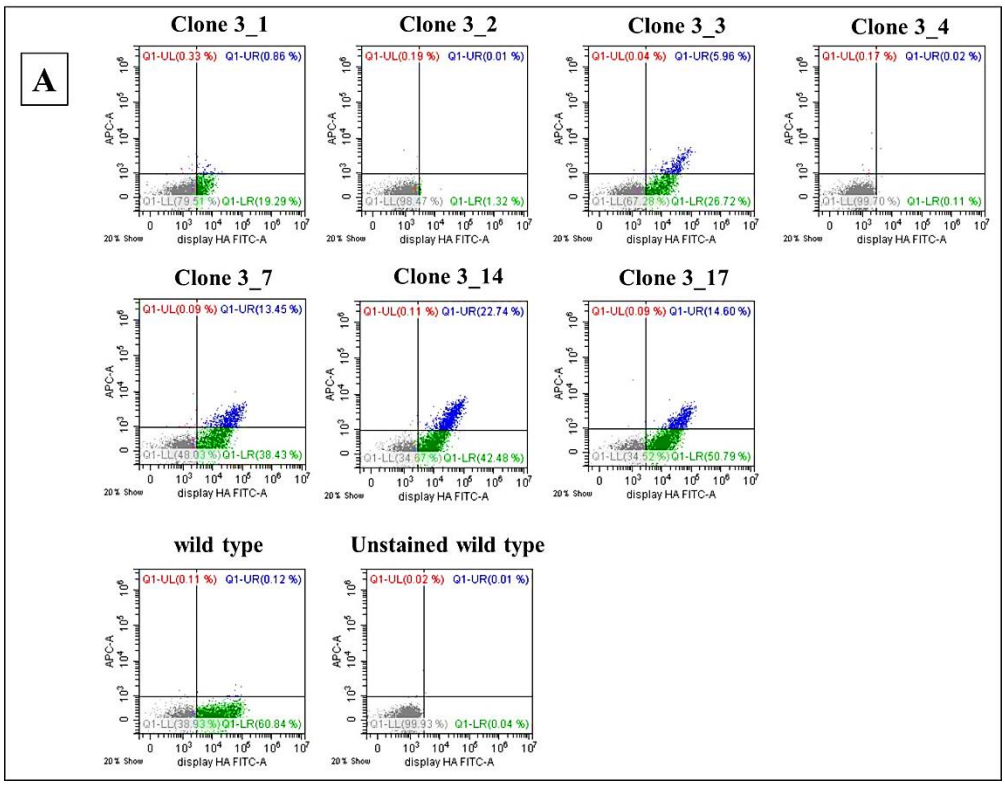

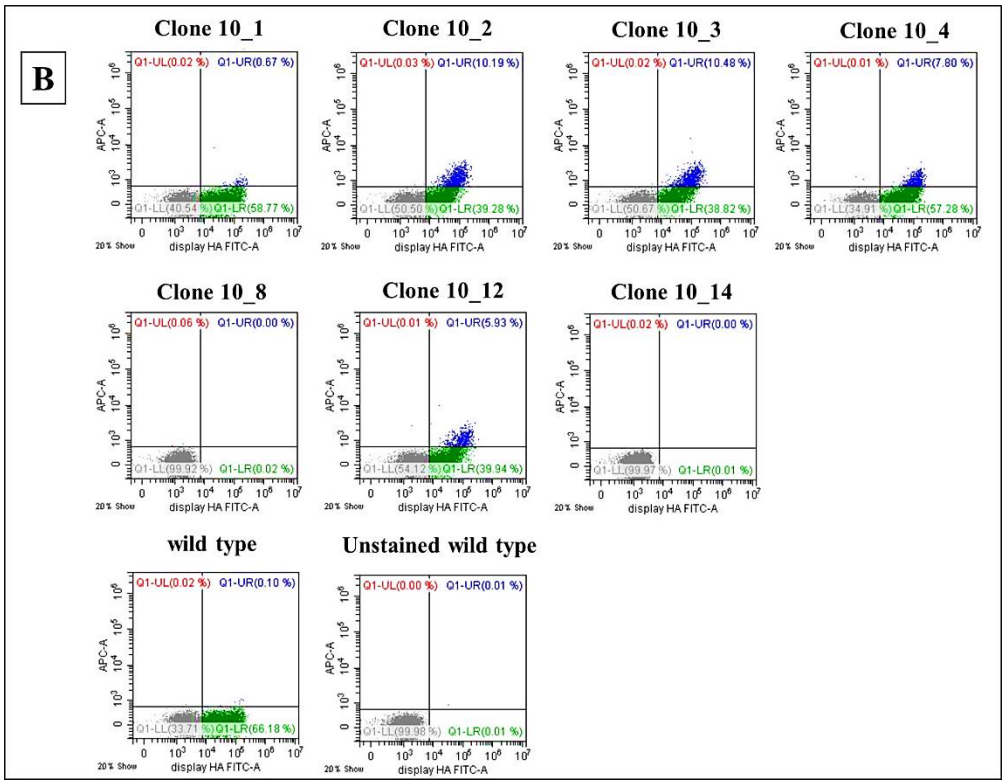

Fig. 20: binding assay of PD-L1 protein to the different mutated yeast clones identified by Sanger sequencing. The mutated clones selected from the two libraries were tested at 10 pM PD-L1 in two independent experiments (library 3 in panel A and library 10 in panel B) in comparison with the wild type clone. 4 out of the 7 different mutated clones identified from each library had an improved binding compared to the wild type (Q1-UR quadrants). The fluorescence thresholds were fixed using an unstained control (shown only for wild type yeast, because it was the same for all clones).

4.10. Characterization of the individual yeast-scFv clones

To estimate the magnitude of the binding improvement of all the different mutated yeast-scFv clones positive to the screening in fig. 20 (6 different clones overall), binding curves to recombinant PD-L1 protein were performed. The induced mutated and wild type clones were tested at the same antigen concentrations as in fig. 16 (ranging from 10 pM to 30 nM) and the yeast-antigen complexes were analyzed by flow cytometry. To avoid that the display level of each scFv could influence the result, the mean fluorescence intensity related to the binding level of the yeast-PD-L1 complexes (double positive cells in fig. 3) was normalized to the mean fluorescence intensity of their display level and the ratio was plotted as a function of the antigen concentration, as shown in the graph in fig. 21. The half-saturating antigen concentration (corresponding to the apparent Kd) of each clone was estimated and all the values were in the low nanomolar range (< 1nM, fig. 21). They corresponded to a 6,3-fold to a 9,8-fold binding improvement compared to the wild type clone, thus confirming that these mutated scFvs really bound to PD-L1 with a higher affinity in this yeast display system. The two clones common to both the libraries were tested twice (i.e. a copy coming from each library) but, as the result was the same, only the copy coming from library 3 is shown (clones 3_3 and 3_14).

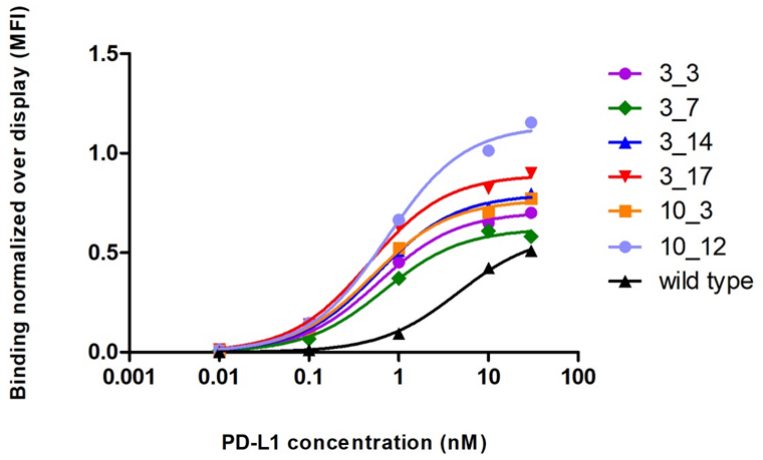

clone name	Kd (nM)	fold change compared to wild type
3_3	0,60	7,6
3_7	0,68	6,7
3_14	0,58	7,9
3_17	0,46	9,8
10_3	0,50	9,0
10_12	0,73	6,3
wild type	4,55	1,0

Fig. 21: titration curves of the individual yeast-scFv clones to PD-L1 antigen. The half-saturating antigen concentration was determined for all the different clones, which were able to bind to the limiting antigen concentration (fig. 20). The Kd values and their relative binding improvement (as fold change compared to the wild type) are reported in the table. For the clones in common to libraries 3 and 10 (table 4), only the copy from library 3 is shown (clones 3_3 and 3_14).

		CDR3 amino acid position											display	binding at limiting PD-L1 concentration	number of copies	relative affinity (fold change compared to wild type)
		1	2	3	4	5	6	7	8	9	10	11				
	wild type	T	K	W	E	L	V	D	P	Y	D	Y				
library 3	clone 3_1	A	K	W	E	L	V	D	P	Y	D	Y	low	no	1	/
	clone 3_2	S	K	W	E	L	V	D	P	Y	D	Y	no	no	4	/
	clone 3_3	S	K	W	E	L	V	D	P	Y	N	Y	high	yes	2	7,6
	clone 3_4	T	K	W	E	L	V	D	P	Y	Y	Y	no	no	1	/
	clone 3_7	S	K	W	E	L	V	D	P	Y	Y	Y	high	yes	1	6,7
	clone 3_14	S	K	W	E	L	V	D	P	Y	G	Y	high	yes	7	7,9
	clone 3_17	S	K	W	E	L	V	D	P	Y	A	Y	high	yes	2	9,8
library 10	clone 10_1	T	K	W	E	L	V	D	P	F	D	Y	high	no	2	/
	clone 10_2	S	K	W	E	L	V	D	P	Y	G	Y	high	yes	9	7,9
	clone 10_3	S	K	W	E	L	V	D	P	F	G	Y	high	yes	3	9
	clone 10_4	S	K	W	E	L	V	D	P	Y	N	Y	high	yes	6	7,6
	clone 10_8	T	K	W	E	L	V	D	P	F	N	Y	no	no	2	/
	clone 10_12	S	K	W	E	L	V	D	P	Y	G	N	high	yes	1	6,3
	clone 10_14	T	K	W	E	L	V	D	P	F	G	Y	no	no	1	/

Table 5: summary of all the different mutated scFvs identified from sequencing analysis. For each clone, besides the sequence of the CDR3, various features are reported: presence or absence of display and binding to limiting PD-L1 concentrations, enrichment level and relative binding improvement (calculated only for clones positive to limiting PD-L1 concentrations).

4.11. Generation, expression and purification of D25 full-length IgGs

The sequences of the wild type and mutated scFvs expressed by the yeast clones showing an affinity improvement were converted into full length IgGs type 4 and then expressed in a mammalian cell system, as described in the methods. These IgGs were subsequently purified from the culture medium of the host cells and, in order to check the purity, molecular weight and proper assembly of the mAbs, SDS-PAGE in reducing and not reducing conditions followed by Coomassie staining were performed.
As shown in fig. 22A, after SDS-PAGE in reducing conditions only two bands were present in the purified preparations of the mAbs selected from the library 3; the molecular weights (27 and 50 kDa, respectively) of the bands corresponded exactly to those of the antibody heavy and light chains, thus confirming the identity of the molecules and the purity of all the preparations. Moreover, these chains were properly assembled to form mature IgGs, as demonstrated by the presence of the expected-molecular weight band of about 150 kDa (two light plus two heavy chains) observed after the not reducing SDS-PAGE (fig. 22B).

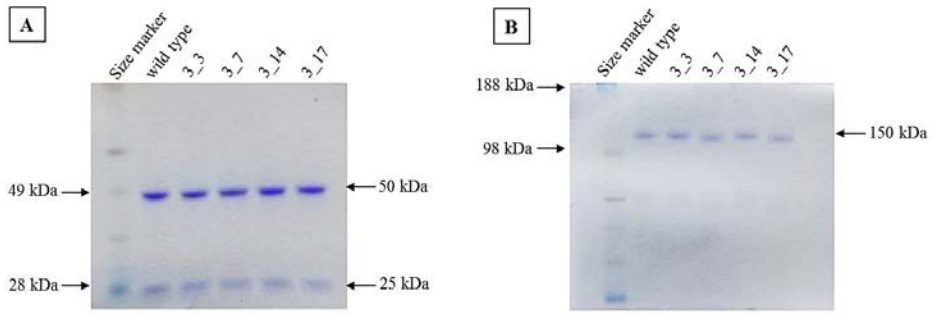

Fig. 22: SDS-PAGE of the purified mAbs and subsequent Coomassie staining. The purified preparations of the converted mAbs were analyzed by SDS-PAGE in reducing (panel A) and not reducing (panel B) conditions. At the top of each lane, the name of the mAb is indicated. The molecular weights on the left correspond to the reference bands of the size marker, while those on the right indicate the size of the bands present in the tested samples.

4.12. Binding assays of the mutated IgGs to hPBMCs

To assess whether the mutated IgGs from the library 3 were able to bind PD-L1 protein with a higher affinity than the wild type as their corresponding scFvs, binding curves of all these mAbs were performed to human activated lymphocytes. Human PBMCs from healthy donors were activated with anti-CD3/CD28 beads to stimulate PD-L1 expression (fig. 23A), then bound to a wide range of IgG concentrations and analyzed by flow cytometry.

All these mAbs bound only to activated lymphocytes, thus confirming that the mutagenesis had not changed the PD-L1 binding specificity in comparison with the wild type IgG (fig. 23B). To determine their apparent affinity constants, the mean fluorescence intensity of PD-L1-binding lymphocytes was plotted against the antibody concentration (fig. 24); the Kd values were in the subnanomolar range and they were two-fold higher than the wild type IgG, except for mAb number 3_7, which showed almost no affinity improvement.

In addition, the percentage of PD-L1-binding cells at not saturating IgG concentrations (240 pM, 48 pM, 9,6 pM) was significantly higher for the mutated mAbs (3_3, 3_14, 3_17) than the wild type one, as reported in table 5.

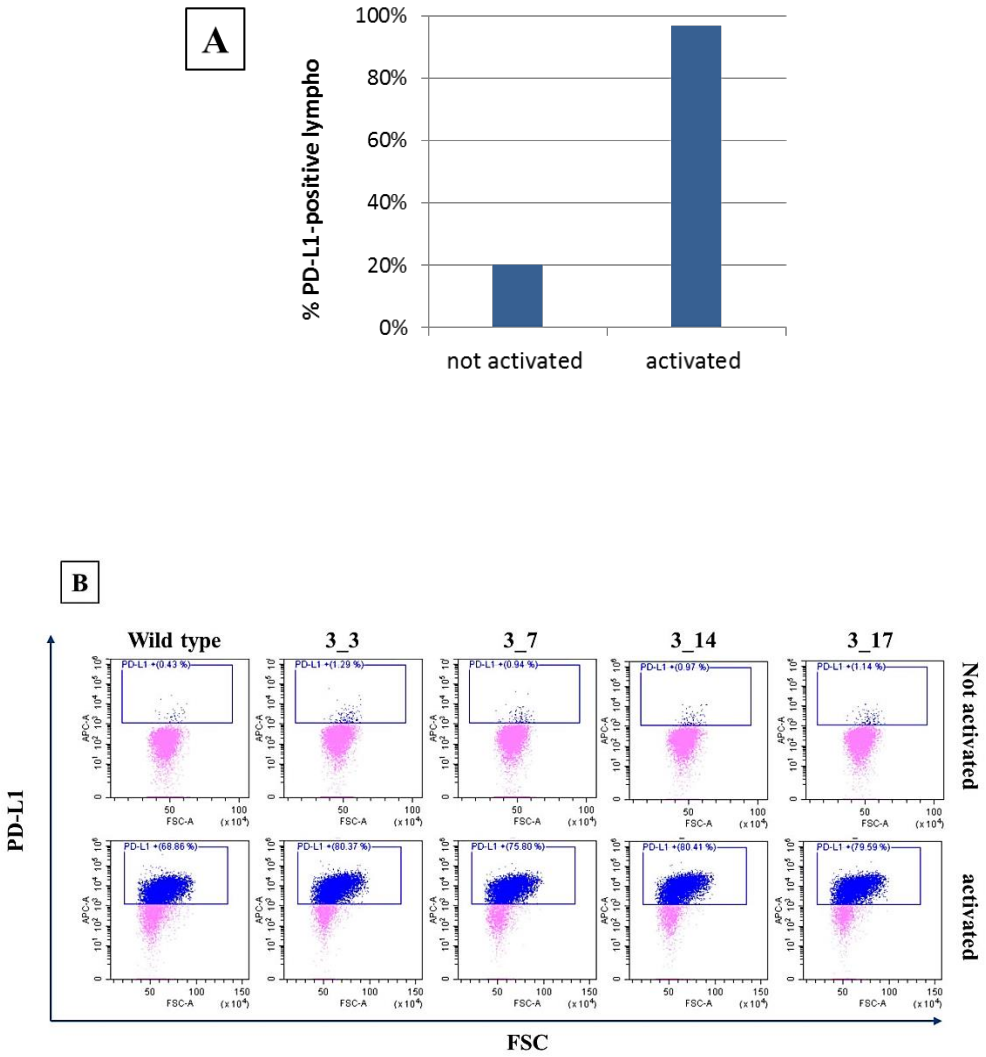

Fig. 23: evaluation of PD-L1 specificity of the converted IgGs. In panel A, the increase in PD-L1 expression upon PBMC activation, detected with a commercial anti PD-L1 antibody, is shown and expressed as percentage of PD-L1-positive cells. In panel B, the percentages of PD-L1-positive lymphocytes obtained at a saturating concentration of 6 nM (fig. 24) of all the IgGs are shown (blue cells) for both not activated (upper panels) and activated (lower panels) cells.

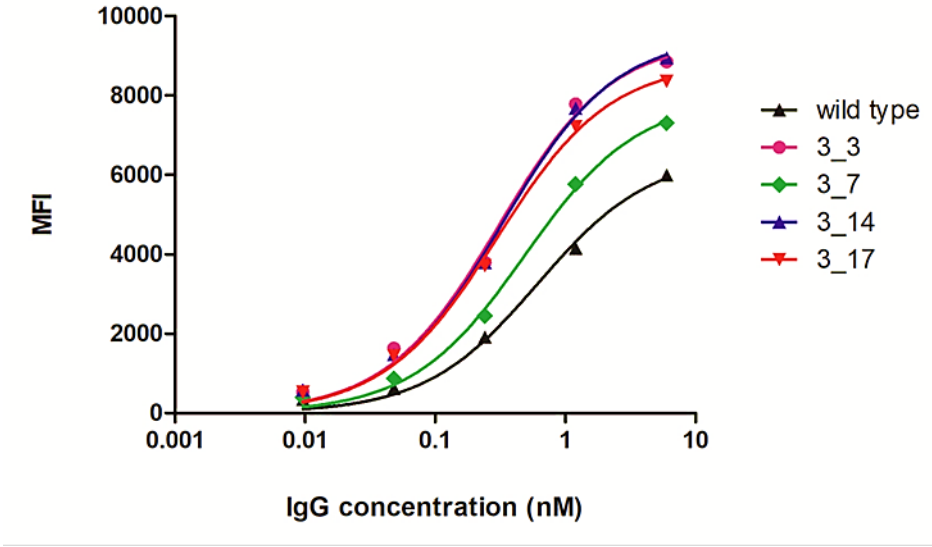

	Kd (nM)	fold change compared to wild type
wild type	0,6128	1,0
3_3	0,3058	2,0
3_7	0,4879	1,3
3_14	0,3245	1,9
3_17	0,2991	2,0

Fig. 24: binding curves of the IgGs from library 3 to hPBMCs. In the graph above, the binding curves of all the IgGs are shown in the same color as their own corresponding scFvs in fig. 21. The half-saturating antigen concentrations (Kd) are reported in the table, in comparison with the wild type IgG.

IgG conc. / IgG name	6 nM	1,2 nM	240 pM	48 pM	9,6 pM
wild type	68,9%	58,5%	39,4%	9,6%	0,7%
3_3	80,4%	78,6%	64,6%	38,6%	5,4%
3_7	75,8%	71,9%	53,9%	18,3%	0,9%
3_14	80,4%	77,0%	64,2%	33,8%	6,8%
3_17	79,6%	77,9%	60,9%	34,2%	4,4%

Table 5: percentages of PD-L1-positive lymphocytes after binding of the IgGs. The table shows the percentages of activated lymphocytes that bound to the different concentrations (first raw) of the library 3 IgGs (indicated in the first column), in comparison with the wild type one. The binding assay is the same as that indicated in fig. 24.

5. DISCUSSION

Monoclonal antibodies (mAbs) have proven to be versatile therapeutic tools for the treatment of several disorders and, due to their potentials such as the extreme target selectivity, their discovery is in constant development. Along with the identification of novel lead antibodies, many progresses have been done in antibody engineering in order to improve their therapeutic efficacy and safety profile (Igawa et al, 2011). In particular, the maturation of the antibody affinity is crucial to ensure high efficacy and it is achieved by means of *in vitro* technologies that allow to obtain antibodies with picomolar affinities. Yeast surface display (YSD) is the most widely used and powerful approach, taking advantage from an efficient library generation by *in vivo* yeast recombination and from the FACS-based isolation of improved antibody variants (Chao et al, 2006; Gera et al, 2013).

Many antibodies are used in cancer immunotherapy; in this field, besides the traditional approaches, in which monoclonal antibodies are used for the direct targeting and subsequent killing of cancer cells (Chiavenna et al, 2017), a novel and successful antibody-based approach has emerged. This strategy aims to the re-activation of the anti-tumor immune response, which is often inhibited by several immune escape mechanisms exploited by cancer cells. Many human solid tumors and hematological malignancies upregulate PD-L1, a component of the immune checkpoints involved in the blockade of the immune response; upon binding to its receptor PD-1 expressed on T cell surface, PD-L1 activates the immune checkpoint signaling in tumor infiltrating T lymphocytes, suppressing the T cell-mediated antitumor immunity. The targeting of the immune checkpoint pathways with blocking antibodies or alternative antibody formats, directed against the receptors and their ligands, is a promising approach in cancer immunotherapy (Pennock et al, 2015).

In this study, we described an optimization of the YSD methodology focused on the set up of a faster and more effective protocol for the generation of novel high affinity single chain antibody fragments (scFv) targeting PD-L1.

The affinity maturation started from the sequence of a new anti PD-L1 scFv (named D25), previously identified in our lab by phage display technology (unpublished data). We used a CDR-targeted mutagenesis protocol involving only the heavy chain variable region CDR3, which represented a very small region (33 bp in lenght) of the whole scFv (735 bp). This choice was based on a comparative sequence analysis between D25 and many other scFvs of the same phagemid library which D25 came from; this study revealed that the variability was located only in the CDR3s, while all the rest of VH, included the CDR1 and CDR2, were identical in all the analyzed scFvs, for this reason we hypothesized that these constant regions could play a scaffold role in all

these antibody fragments and we kept them unmodified. In addition, it is well known that CDR3s of VH and VL tend to dominate the antibody-antigen interactions, generally making more extensive contacts than the other CDRs (Sundberg et al, 2002).

Our first objective was to generate a library in which most of the sequences carried missense mutations in the CDR3, reducing the wild type sequences and those containing stop codon mutations; because in a single-step error-prone PCR we did not obtain a frequency of mutants higher than 25-30%, we set up a protocol based on repeated mutagenesis cycles on the same target sequence. Moreover, we provide a systematic analysis, performed by high-throughput sequencing, of the mutation frequencies occurring in the CDR3 over ten subsequent error-prone PCR cycles, suggesting a model that could be generally applied to any target sequence.

As a proof of the effectiveness of this approach, we evaluated the nucleotide wild type frequency and we found out a progressive, but not linear reduction of the wild type percentage, which were just 5% of the total sequences at the last mutagenesis cycle. These data were very meaningful but not completely informative for our purpose, so we subsequently focused on the analysis of the amino acid sequences; we observed the same progressive decrease of the wild type amino acid sequences throughout the 10 rounds, but the percentage of amino acid wild type sequences exceeded (of about 5-10%) that of the nucleotide wild type at each round, probably due to those sequences that contained only silent mutations. The increase of mutated sequences throughout the mutagenesis cycles followed a non-linear trend, indicating that the mutation rate was not constant at each cycle (fig. 13). Clearly, during the earliest mutagenesis rounds the chance to transform a wild type sequence in a mutated one was the highest possible, as demonstrated by the 40% drop of the wild type CDR produced by the first round alone (fig. 13); on the contrary, when the mutagenesis cycles proceeded, the wild type template became less frequent and new mutations were more likely to be introduced in previously mutated sequences.

Regarding the quality of the mutated sequences, the presence of stop codons is clearly considered “bad”, representing the clones that are likely to be lost during FACS-based selections because, encoding for truncated proteins, should be unable to bind the antigen or even not displayed. Interestingly, stop codon mutations were introduced with the same rate at each round (about 2%), determining a linear trend with a peak of 20% at cycle 10.

We made a further characterization in terms of number of mutations per sequence; we expected to accumulate sequences with multiple mutations over the mutagenesis but, considering that the CDR3 consisted only in 11 amino acids, too many mutations could have a negative impact on scFv-antigen binding. Mutants with a single amino acid substitution had a peak at cycle 1

(57% of sequences carrying missense mutations) and decreased in a linear fashion at cycle 10 (28%). This trend was the consequence of the accumulation of additional mutations that progressively reduced the abundance of single mutants, while increasing that of double, triple ones and so on. Sequences with more than 4 mutations, which were analyzed as a single class, represented a considerable fraction (20%) already at round 1, but fortunately they showed only a slight increase up to the end of mutagenesis (fig. 14).

In the light of all the previous analyses, the CDR3 pool of mutants obtained after 10 mutagenesis rounds had the desired features, in fact reads containing missense mutations were more than two thirds of the pool (70%) and the wild type percentage was the least among all the cycles (10%). In addition, at round 10 the percentages of double and triple mutants were the highest of all rounds (28% and 15%, respectively, fig. 14). Sequences containing stop codons were not so rare (20% of the total sequences), but fortunately the detection system of the yeast-antigen complexes automatically excluded these clones from selection. However, according to our goal of setting up a fast and more effective affinity maturation protocol, we evaluated whether it is essential to perform so many rounds of error-prone PCR to obtain a high quality scFv library. Therefore, besides the generation of a library coming from mutated fragments obtained at cycle 10, we generated another library using fragments from mutagenesis cycle 3, in order to test if a 50% frequency of sequences with missense mutations was sufficient for our purposes (fig. 13).

Although the above analysis is referred to the error-prone PCR fragments, we assumed that the generated yeast-scFv libraries should maintain the same features as the mutated fragments (3 and 10) used to construct them.

We achieved theoretical complexities of 2×10^8 and $1{,}7 \times 10^8$ for the libraries 3 and 10 , respectively, and considering that the fractions of mutants in the corresponding CDR3 pools were 50% and 70%, more or less 1×10^8 and $1{,}2 \times 10^8$ clones, respectively, should be “good” clones. These are considered optimal starting complexities to ensure an efficient and successful isolation of high affinity variants (Chao et al, 2006; Gera et al, 2013).

Although we also knew the percentages of single and multiple mutants (double, triple, etc) in the sequences with missense mutations (fig. 14), we could not exactly foresee if they included all the possible single amino acid mutations and all the combinations of multiple substitutions. In fact, some amino acid mutations were less likely to occur than others, i.e. when two or even three nucleotide changes in the same codon were required. However, considering the huge number of missense mutation in the libraries and the short length of the target sequence (11 aa), we postulated that the CDR3 of the wild type scFv D25 is highly randomized.

The different selection schemes adopted for the two libraries shared essentially a common strategy, i.e. the use of saturation concentrations of antigen (30 or 10 nM) in the first FACS selection step and, by contrast, a very low concentration (10 pM) in the last one. The limiting antigen concentration, used to avoid the selection of the wild type clones present in the library, was chosen as concentration in which the wild type yeast didn't bind to PD-L1 antigen in a binding curve experiment (fig. 16B). In this way, in the last step of FACS selection, very few events were sorted (only 75 clones from library 3 and 900 from library 10) at the expense of the diversity of the selected population, but increasing the chance to catch the top binders only. Such a strategy substantially differed from the others so far reported in literature, where the concentrations of the soluble antigen gradually decreased from a round to another (Chao et al, 2006).
The same limiting antigen concentration was also used for a rapid binding test on the sorted population, in order to establish if it was necessary to go on or to stop the selection. The strong double positive signal of the sorted populations compared to the wild type (fig. 19) strongly suggested the presence of several clones with improved binding capacity among the selected yeasts.
Sanger sequencing was performed on 24 clones, randomly chosen after the bulk amplification of the sorted cells from libraries 3 and 10, and 12 different clones were identified overall (table 5). As previously made for the whole sorted population, each individual clone was tested with the limiting PD-L1 concentration; this binding assay confirmed that 6 out of 12 clones (clones 3_3, 3_7, 3_14, 3_17 from library 3 and clones 10_3 and 10_12 from library 10) were really able to bind to PD-L1 better than the wild type yeast clone. Their relative affinity improvement compared with the wild type, estimated by titration curves to PD-L1 antigen, was between 6,3 and 9,8 fold (fig. 21 and table 5). Interestingly, most of these scFvs (3_3, 3_14, 3_17 in fig. 24) maintained a certain affinity improvement (2-fold higher than the wild type) when converted into whole antibodies and tested on PD-L1 in its physiological environment, that is expressed on the plasma membrane of activated hPBMCs.
Although a very limited number of clones was sampled, their features reflected both the differences of the respective parental libraries and the different sorting strategies used to select them. Firstly, no wild type clones were found among the sorted yeasts from library 10 compared to library 3 (25% of sorted wild type); in our opinion, this depended on both the lower wild type starting frequency of library 10 compared to 3 (10% *versus* 43%) and the higher sorting gate stringency applied since the first step of library 10 selection (fig. 17 and 18). Secondly, only single and double mutants were obtained from library 3, while some triple mutants were selected too from

library 10, reflecting the higher abundance of such kind of mutants in this library (three-fold higher at round 10 than round 3). Moreover, no stop codon clones were found, although they were not so rare in the parental libraries (10% and 20%, from libraries 3 and 10, respectively), demonstrating the efficiency of labelling the C-term of the scFvs to distinguish the full-length proteins from the truncated ones.

By a comparison of the two groups of selected clones, we observed that mutations always affected the same CDR3 amino acid positions (the first and the tenth ones), in addition to another position (the ninth amino acid) which was mutated in 33% of the scFvs selected from library 10 (table 3 and 4). A more interesting observation was that the amino acid substitutions were the same in the two libraries, in fact the Thr (T) in position 1 was always replaced by a Ser (S); similarly, the Asp (D) in position 10 was always turned into a Gly (G) or an Asn (N), less frequently into an Ala (A) or a Tyr (Y) (clones from library 3). Remarkably, two double mutant clones were common to both sorted yeast populations (S+G and S+N mutant, i.e. clones 3_3 and 3_14, corresponding to clones 10_4 and 10_2, respectively) and one of them (S+G) was the most enriched clone. Thus, it is clear that the mutated positions in the selected clones were true hotspots and these results were of great relevance considering that the library features and the selection schemes were a little different in the two cases.

By observing the sequences of the best binder yeast clones (table 5), we noticed that they included all the double mutants with substitutions in the first and tenth positions (clones 3_3, 3_7, 3_14, 3_17, 10_2 and 10_4) and the two triple mutants (clones 10_3 and 10_12). Interestingly, two of the three amino acid substitutions found in these triple mutant scFvs were the same as those present in the double mutant 3_14. Moreover, we found out a sort of direct correlation between the enrichment level of these clones and their relative binding capacity improvement; consistently, the two clones present in single copy (clones 3_7 and 10_12) showed a lower relative improvement compared with all the others, which were present in more than one copy (from 2 to 9 copies per library, table 5).

Unexpectedly, there were some sorted clones (all the single mutants and two kinds of double mutants) which were not able to display their scFvs (fig. 20) or, in some cases, did not have an improved binding (clone 10_1). However, they were not highly enriched (one or two copies at most), supporting the idea that they were accidentally sorted; we hypothesized that, due to a little and occasional background of the fluorescent antibodies on some not-displaying yeasts, these clones could fall in the double positive quadrant although they did not really bind to the antigen.

It seemed that some single mutations had detrimental effects, which were reverted by coupling them to other specific substitutions in a precise position,

maybe having a compensatory function. For example, the S at the first amino acid did not allow scFv display (clone 3_2, fig. 20) but, when S was coupled with one of the substitutions found at the tenth position, the display was restored and affinity was even improved (clones 3_3, 3_7, 3_14, 3_17, table 5). Another example was the F at the ninth position: when alone, it did not change a lot scFv binding affinity to PD-L1 compared to wild type (clone 10_1, fig. 20), but the combination with a mutation at the near tenth position even abolished the display (clone 10_8 and 10_14). Surprisingly, the triple mutant scFv, containing these two mutations plus the S at the first position, had an improved binding affinity (clone 10_3).

Taken together, these observations suggested that some mutation hotspots were present in the CDR3, most of which were identified independently from the number of mutagenesis rounds performed on the CDR3 and from the number of sorting rounds used to select the high affinity scFvs.

The overall affinity improvement of the clones (6,3 to 9,8 fold) can be considered, in our opinion, a good achievement for various reasons: firstly, the wild type clone has already a high antigen affinity (low nanomolar, fig. 21) for its target, then the number of selection cycles performed and the number of sequenced clones was limited. Obviously, performing high-throughput sequencing of sorted clones could help to search for other good candidates, in addition to those ones identified by the small sampling described here.

According to our objective of isolating novel full length mAbs for cancer immunotherapy, all the scFvs were converted into IgGs to evaluate if this format maintained the same affinity improvement as the single chain. Only the IgGs isolated from the library 3 have been tested so far and 3 out of 4 mAbs (3_3, 3_14, 3_17 in fig. 24) showed an affinity improvement in comparison with the wild type mAb, although it was not of the same entity (2-fold higher affinity) as that of the corresponding scFvs. In our opinion this phenomenon could be due either to the conversion of a monovalent format (scFv) into a bivalent one (whole mAb) or to the fact that the IgGs were tested on a PD-L1 antigen in its biological context, while the scFvs were selected using a soluble PD-L1 protein. Nevertheless, there was some consistency between the data obtained in the two systems, in fact the scFv-yeast with the lowest antigen affinity (clone 3_7 in fig. 21) was the worst when converted into IgG and tested on PBMCs (fig. 24).

The real amelioration of the mutated IgG affinity *versus* the wild type one was also proven by the increase of the percentages of PD-L1 positive cells obtained at not saturating concentrations of the mutated mAbs (table 5); in particular, the lowest the Ab concentration, the highest was the difference between mutated and wild type mAbs.

6. CONCLUSIONS

We set up a fast antibody CDR affinity maturation protocol by yeast display and we succeeded in isolating novel high affinity anti PD-L1 scFv-yeast clones with a 6,3- to 9,8-fold affinity improvement compared with the parental scFv. These antibody fragments could be very good candidates for an antibody-based, PD-L1-targeted cancer immunotherapy, since they maintained an affinity improvement when converted into whole mAbs and tested in a more physiological environment, that is when PD-L1 is expressed on the plasma membrane.

The features of the starting yeast library are crucial to determine the success of the affinity maturation and we have learnt from our previous experience that a great fraction of wild type sequences in the parental library can make the search for high affinity mutants a very difficult and slow procedure. We developed a protocol that, performing just 3 mutagenesis rounds, halved the wild type percentage, ensuring in the meantime a good heterogeneity of the pool of mutants. Moreover, we proposed a selection strategy that has never been reported in yeast display protocols found in literature to date: after a first sorting round performed with saturation antigen concentrations, as usually suggested to avoid loss of rare but high affinity mutants, a second round was performed, using a very low antigen concentration which was not able to bind the wild type clone. This two-step, high-low antigen concentration approach, used to “hide” the wild type clones present in the library, represents the novelty of our selection scheme and, although it was likely to cause loss of several good clones, it granted a rapid isolation of some improved scFvs. In addition, we demonstrated that, by coupling an efficient mutagenesis to a stringent selection, it was not necessary to make a deep sequencing analysis of the selected clones to identify mutants with improved affinity.

The characterization of the mAbs isolated in this study is to be completed by testing the IgGs selected from library 10 on hPBMCs. However, to collect additional binding data for a full understanding of the association and dissociation kinetics of these antibodies from the antigen, surface plasmon resonance (SPR) studies have been planned.

In vitro and *in vivo* assays are necessary to evaluate the efficacy of the novel mAbs. As for the *in vitro* studies, we will investigate the inhibition of PD-L1 pathway at a molecular level and we will measure the inhibition of the proliferation of activated hPBMCs by quantifying the IL-2 secreted in the culture medium upon treatment with various concentrations of the mutated and wild type mAbs.

The *in vivo* potency of the novel mAbs will be assessed in mice with established tumors by determining the ability of the antibodies to induce the regression/remission of.the tumor in comparison with the wild type.

7. REFERENCES

Alpan RS, Zhang M, Pardee AB. Cell cycle-dependent expression of TAP1, TAP2, and HLA-B27 messenger RNAs in a human breast cancer cell line. *Cancer Research* (1996) 56(19):4358–4361.

Ansell SM, Lesokhin AM, Borrello I, Halwani A, Scott EC, Gutierrez M, Schuster SJ, Millenson MM, Cattry D, Freeman GJ, Rodig SJ, Chapuy B, Ligon AH, Zhu L, Grosso JF, Kim SY, Timmerman JM, Shipp MA, Armand P. PD-1 blockade with nivolumab in relapsed or refractory Hodgkin's lymphoma. *New England Journal of Medicine* (2015) 372(4):311–9.

Antonia SJ, López-Martin JA, Bendell J, Ott PA, Taylor M, Eder JP, Jäger D, Pietanza MC, Le DT, de Braud F, Morse MA, Ascierto PA, Horn L, Amin A, Pillai RN, Evans J, Chau I, Bono P, Atmaca A, Sharma P, Harbison CT, Lin CS, Christensen O, Calvo E. Nivolumab alone and nivolumab plus ipilimumab in recurrent small-cell lung cancer (CheckMate 032): a multicentre, open-label, phase 1/2 trial. *Lancet Oncology* (2016) 17(7):883-95.

Azuma T, Yao S, Zhu G, Flies AS, Flies SJ, Chen L. B7-H1 is a ubiquitous antiapoptotic receptor on cancer cells. *Blood* (2008) 111(7): 3635–43.

Barderas R, Desmet J, Timmerman P, Meloen R, Casal JI. Affinity maturation of antibodies assisted by in silico modeling. *Proceedings of the National Academy of Sciences USA* (2008) 105:9029-34.

Batista FD, Neuberger MS. Affinity dependence of the B cell response to antigen: a threshold, a ceiling and the importance of off-rate. *Immunity* (1998) 8:751-9.

Benatuil L, Perez JM, Belk J, Hsieh CM. An improved yeast transformation method for the generation of very large human antibody libraries. *Protein Eng Des Sel* (2010) 23(4):155-9.

Boder ET, Midelfort KS, Wittrup KD. Directed evolution of antibody fragments with monovalent femtomolar antigen-binding affinity. *Proceedings of the National Academy of Sciences USA* (2000) 97:10701-5.

Buonpane RA, Churchill HR, Moza B, Sundberg EJ, Peterson ML, Schlievert PM, Kranz DM. Neutralization of staphylococcal enterotoxin

B by soluble, high-affinity receptor antagonists. *Nature Medicine* (2007) 13(6):725-9.

Buonpane RA, Moza B, Sundberg EJ, Kranz DM. Characterization of T cell receptors engineered for high affinity against toxic shock syndrome toxin-1. *Journal of Molecular Biology* (2005) 353(2):308-21.

Campadelli-Fiume G, Petrovic B, Leoni V, Gianni T, Avitabile E, Casiraghi C, Gatta V. Retargeting Strategies for Oncolytic Herpes Simplex Viruses. *Viruses* (2016) 8(3):63.

Carter P. Improving the efficacy of antibody-based cancer therapies. *Nature Reviews Cancer* (2001) 1(2):118-29.

Casadevall A, Dadachova E, Pirofski LA. Passive antibody therapy for infectious diseases. *Nature Reviews Microbiology* (2004) 2(9):695-703.

Chan AC, Carter PJ. Therapeutic antibodies for autoimmunity and inflammation. *Nature Reviews Immunology* (2010) 10:301–16.

Chang CH, Curtis JD, Maggi LB Jr, Faubert B, Villarino AV, O'Sullivan D, Huang SC, van der Windt GJ, Blagih J, Qiu J, Weber JD, Pearce EJ, Jones RG, Pearce EL. Posttranscriptional control of T cell effector function by aerobic glycolysis. *Cell* (2013) 153(6):1239–51.

Chao G, Lau WL, Hackel BJ, Sazinsky SL, Lippow SM, Wittrup KD. Isolating and engineering human antibodies using yeast surface display. *Nature Protocols* (2006) 1(2):755-68.

Chen Y, Liu P, Gao F, Cheng H, Qi J, Gao GF. A dimeric structure of PD-L1: functional units or evolutionary relics? *Protein and Cell* (2010) 1(2):153-60.

Chiavenna SM, Jaworski JP, Vendrell A. State of the art in anti-cancer mAbs. *Journal of Biomedical Science* (2017) 24:15.

Cho HY, Lee SW, Seo SK, Choi IW, Choi I, Lee SW. Interferon-sensitive response element (ISRE) is mainly responsible for IFN-alpha-induced upregulation of programmed death-1 (PD-1) in macrophages. *Biochimica and Biophysica Acta* (2008) 1779(12):811–9.

Chowdhury PS, Pastan I. Improving antibody affinity by mimicking somatic hypermutation in vitro. *Nature Biotechnology* (1999) 17(6):568 – 572.

Clark LA, Boriack-Sjodin PA, Eldredge J, Fitch C, Friedman B, Hanf KJM, Jarpe M, Liparoto SF, Li Y, Lugovskoy A, Miller S, Rushe M, Sherman W, Simon K, Van Vlijmen H. Affinity enhancement of an in vivo matured therapeutic antibody using structure-based computational design. *Protein Science* (2006) 15:949-60.

Clynes RA, Towers TL, Presta LG, Ravetch JV. Inhibitory Fc receptors modulate in vivo cytotoxicity against tumor targets. *Nature Medicine* (2000) 6(4):443-6.

Cochran JR, Kim YS, Lippow SM, Rao B, Wittrup KD. Improved mutants from directed evolution are biased to orthologous substitutions. *Protein Eng Des Sel* (2006) 19(6):245-53.

Crane CA, Panner A, Murray JC, Wilson SP, Xu H, Chen L, Simko JP, Waldman FM, Pieper RO, Parsa AT. PI(3) kinase is associated with a mechanism of immunoresistance in breast and prostate cancer. *Oncogene* (2009) 28(2):306–12.

Dam J, Guan R, Natarajan K, Dimasi N, Chlewicki LK, Kranz DM, Schuck P, Margulies DH, Mariuzza RA. Variable MHC class I engagement by Ly49 natural killer cell receptors demonstrated by the crystal structure of Ly49C bound to H-2K(b). *Nature Immunology* (2003) 4(12):1213-22.

Di Noia JM, Neuberger MS. Molecular mechanisms of antibody somatic hypermutation. *Annual Review of Biochemistry* (2007) 76:1–22.

Doerner A, Rhiel L, Zielonka S, Kolmar H. Therapeutic antibody engineering by high efficiency cell screening. *FEBS Letters* (2014) 588: 278–287.

Dunn GP, Bruce AT, Ikeda H, Old LJ, Schreiber RD. Cancer immunoediting: From immunosurveillance to tumor escape. *Nature Immunology* (2002) 3:991–998.

Fife BT, Bluestone JA. Control of peripheral T-cell tolerance and autoimmunity via the CTLA-4 and PD-1 pathways. *Immunological Reviews* (2008) 224:166–182.

Foote J, Eisen HN. Kinetic and affinity limits on antibodies produced during immune responses. *Proceedings of the National Academy of Sciences USA* (1995) 92:1254-6.

Freeman GJ, Wherry EJ, Ahmed R, Sharpe AH. Reinvigorating exhausted HIV-specific T cells via PD-1-PD-1 ligand blockade. *Journal of Experimental Medicine* (2006) 203(10):2223–7.

Fruci D, Benevolo M, Cifaldi L, Lorenzi S, Lo Monaco E, Tremante E, Giacomini P. Major histocompatibility complex class I and tumour immuno-evasion: how to fool T cells and natural killer cells at one time. *Current Oncology* (2012) 19(1):39–41.

Gabrilovich DI, Nagaraj S. Myeloid-derived suppressor cells as regulators of the immune system. *Nature Reviews Immunology* (2009) 9:162–74.

Gabrilovich DI, Ostrand-Rosenberg S, Bronte V. Coordinated regulation of myeloid cells by tumours. *Nature Reviews Immunology* (2012) 12(4):253–268.

Garon EB, Rizvi NA, Hui R, Leighl N, Balmanoukian AS, Eder JP, Patnaik A, Aggarwal C, Gubens M, Horn L, Carcereny E, Ahn MJ, Felip E, Lee JS, Hellmann MD, Hamid O, Goldman JW, Soria JC, Dolled-Filhart M, Rutledge RZ, Zhang J, Lunceford JK, Rangwala R, Lubiniecki GM, Roach C, Emancipator K, Gandhi L. Pembrolizumab for the treatment of non-small-cell lung cancer. *New England Journal of Medicine* (2015) 372(21):2018–28.

Gatto D, Brink R. The germinal center reaction. *Journal of Allergy and Clinical Immunology* (2010) 126(5):898 – 907.

Gera N, Hussain M, Rao BM. Protein selection using yeast surface display. *Methods* (2013) 60(1):15-26.

Herbst RS, Soria JC, Kowanetz M, Fine GD, Hamid O, Gordon MS, Sosman JA, McDermott DF, Powderly JD, Gettinger SN, Kohrt HEK, Horn L, Lawrence DP, Rost S, Leabman M, Xiao Y, Mokatrin A, Koeppen H, Hegde PS, Mellman I, Chen DS, Hodi FS. Predictive correlates of response to the anti-PD-L1 antibody MPDL3280A in cancer patients. *Nature* (2014) 515(7528):563–7.

Hey A. History and Practice: Antibodies in Infectious Diseases. *Microbiology Spectrum* (2015) 3(2):AID-0026-2014.

Hodi FS, Chesney J, Pavlick AC, Robert C, Grossmann KF, McDermott DF, Linette GP, Meyer N, Giguere JK, Agarwala SS, Shaheen M, Ernstoff MS, Minor DR, Salama AK, Taylor MH, Ott PA, Horak C,

Gagnier P, Jiang J, Wolchok JD, Postow MA. Combined nivolumab and ipilimumab versus ipilimumab alone in patients with advanced melanoma: 2-year overall survival outcomes in a multicentre, randomised, controlled, phase 2 trial. *Lancet Oncology* (2016) 17:1558–68.

Holliger P, Hudson PJ. Engineered antibody fragments and the rise of single domains. *Nature Biotechnology* (2005) 23(9):1126-36.

Hori J, Wang M, Miyashita M, Tanemoto K, Takahashi H, Takemori T, Okumura K, Yagita H, Azuma M. B7-H1-induced apoptosis as a mechanism of immune privilege of corneal allografts. *Journal of Immunology* (2006) 177(9):5928–35.

https://www.accessdata.fda.gov/scripts/cder/daf/

Igawa T, Tsunoda H, Kuramochi T, Sampei Z, Ishii S, Hattori K. Engineering the variable region of therapeutic IgG antibodies. *MAbs* (2011) 3(3):243-52.

Jin M, Song G, Carman CV, Kim YS, Astrof NS, Shimaoka M, Wittrup DK, Springer TA. Directed evolution to probe protein allostery and integrin I domains of 200,000-fold higher affinity. *Proceedings of the National Academy of Sciences USA* (2006) 103(15):5758-63.

Johnson BF, Clay TM, Hobeika AC, Lyerly HK, Morse MA. Vascular endothelial growth factor and immunosuppression in cancer: current knowledge and potential for new therapy. *Expert Opinion in Biological Therapy* (2007) 7(4):449-60.

Kabat EA. Sequences of Proteins of Immunological Interest (1991) National Institutes of Health Publication No. 91-3242, 5th ed., United States Department of Health and Human Services, Bethesda, MD.

Keir ME, Butte MJ, Freeman GJ, Sharpe AH. PD-1 and its ligands in tolerance and immunity. *Annual Reviews of Immunology* (2008) 26:677–704.

Kinter AL, Godbout EJ, McNally JP, Sereti I, Roby GA, O'Shea MA, Fauci AS. The common gamma-chain cytokines IL-2, IL-7, IL-15, and IL-21 induce the expression of programmed death-1 and its ligands. *Journal of Immunology* (2008) 181(10):6738–46.

Ko BK, Choi S, Cui LG, Lee YH, Hwang IS, Kim KT, Shim H, Lee JS. Affinity Maturation of Monoclonal Antibody 1E11 by Targeted

Randomization in CDR3 Regions Optimizes Therapeutic Antibody Targeting of HER2-Positive Gastric Cancer. *PLoS ONE* (2015) 10(7): e0134600.

Larkin J, Chiarion-Sileni V, Gonzalez R, Grob JJ, Cowey CL, Lao CD, Schadendorf D, Dummer R, Smylie M, Rutkowski P, Ferrucci PF, Hill A, Wagstaff J, Carlino MS, Haanen JB, Maio M, Marquez-Rodas I, McArthur GA, Ascierto PA, Long GV, Callahan MK, Postow MA, Grossmann K, Sznol M, Dreno B, Bastholt L, Yang A, Rollin LM, Horak C, Hodi FS, Wolchok JD. Combined nivolumab and ipilimumab or monotherapy in untreated melanoma. *New England Journal of Medicine* (2015) 373(1):23–34.

Latchman Y, Wood CR, Chernova T, Chaudhary D, Borde M, Chernova I, Iwai Y, Long AJ, Brown JA, Nunes R, Greenfield EA, Bourque K, Boussiotis VA, Carter LL, Carreno BM, Malenkovich N, Nishimura H, Okazaki T, Honjo T, Sharpe AH, Freeman GJ. PD-L2 is a second ligand for PD-1 and inhibits T cell activation. *Nature Immunology* (2001) 2(3):261–8.

Lawrence MS, Stojanov P, Polak P, Kryukov GV, Cibulskis K, Sivachenko A, Carter SL, Stewart C, Mermel CH, Roberts SA, Kiezun A, Hammerman PS, McKenna A, Drier Y, Zou L, Ramos AH, Pugh TJ, Stransky N, Helman E, Kim J, Sougnez C, Ambrogio L, Nickerson E, Shefler E, Cortés ML, Auclair D, Saksena G, Voet D, Noble M, DiCara D, Lin P, Lichtenstein L, Heiman DI, Fennell T, Imielinski M, Hernandez B, Hodis E, Baca S, Dulak AM, Lohr J, Landau DA, Wu CJ, Melendez-Zajgla J, Hidalgo-Miranda A, Koren A, McCarroll SA, Mora J, Crompton B, Onofrio R, Parkin M, Winckler W, Ardlie K, Gabriel SB, Roberts CWM, Biegel JA, Stegmaier K, Bass AJ, Garraway LA, Meyerson M, Golub TR, Gordenin DA, Sunyaev S, Lander ES, Getz G. Mutational heterogeneity in cancer and the search for new cancer-associated genes. *Nature* (2013) 499(7457):214–218.

Lin DY, Tanaka Y, Iwasaki M, Gittis AG, Su HP, Mikami B, Okazaki T, Honjo T, Minato N, Garboczi DN. The PD-1/PD-L1 complex resembles the antigen-binding Fv domains of antibodies and T cell receptors. *Proceedings of the National Academy of Sciences USA* (2008) 105(8):3011–6.

Lipovsek D, Plückthun A. In-vitro protein evolution by ribosome display and mRNA display. *Journal of Immunological Methods* (2004) 290(1-2):51-67.

Liu C, Zhang L, Chang X, Cheng Y, Cheng H, Ye X, Fu T, Chen J, Cui H. Overexpression and Immunosuppressive Functions of Transforming Growth Factor 1, Vascular Endothelial Growth Factor and Interleukin-10 in Epithelial Ovarian Cancer. *Chinese Journal of Cancer Research* (2012) 24(2): 130–137.

Lynch TJ, Bondarenko I, Luft A, Serwatowski P, Barlesi F, Chacko R, Sebastian M, Neal J, Lu H, Cuillerot JM, Reck M. Ipilimumab in combination with paclitaxel and carboplatin as first-line treatment in stage IIIB/IV non-small-cell lung cancer: Results from a randomized, doubleblind, multicenter phase II study. *Journal of Clinical Oncology* (2012) 30(17):2046–2054.

Mahmud N, Klipa D, Ahsan N. Antibody immunosuppressive therapy in solid-organ transplant Part I. *MAbs* (2010) 2(2):148–156.

Marks JD. Antibody affinity maturation by chain shuffling. *Methods in Molecular Biology* (2004) 248:327-43.

Marzec M, Zhang Q, Goradia A, Raghunath PN, Liu X, Paessler M, Wang HY, Wysocka M, Cheng M, Ruggeri BA, Wasik MA. Oncogenic kinase NPM/ALK induces through STAT3 expression of immunosuppressive protein CD274 (PD-L1, B7-H1). *Proceedings of the National Academy of Sciences USA* (2008) 105(52):20852–7.

Maul RW, Gearhart PJ. AID and somatic hypermutation. *Advances in Immunology* (2010) 105:159–91.

Neylon C. Chemical and biochemical strategies for the randomization of protein encoding DNA sequences: library construction methods for directed evolution. *Nucleic Acids Research* (2004) 32(4):1448–1459.

Oda M, Sato-Nakamura N, Azuma T. Molecular characterization of monovalent and multivalent hapten–protein conjugates for analysis of antigen-antibody interaction. *Analytical Biochemistry* (2004) 333(2):365–71.

Pandha H, Rigg A, John J, Lemoine N. Loss of expression of antigen-presenting molecules in human pancreatic cancer and pancreatic cancer cell lines. *Clinical and Experimental Immunology* (2007) 148(1):127–135.

Parry RV, Chemnitz JM, Frauwirth KA, Lanfranco AR, Braunstein I, Kobayashi SV, Linsley PS, Thompson CB, Riley JL. CTLA-4 and PD-1

receptors inhibit T-cell activation by distinct mechanisms. *Molecular and Cellular Biology* (2005) 25(21):9543–9553.

Patsoukis N, Bardhan K, Chatterjee P, Sari D, Liu B, Bell LN, Karoly ED, Freeman GJ, Petkova V, Seth P, Li L, Boussiotis VA. PD-1 alters T-cell metabolic reprogramming by inhibiting glycolysis and promoting lipolysis and fatty acid oxidation. *Nature Communications* (2015) 6:6692.

Patsoukis N, Brown J, Petkova V, Liu F, Li L, Boussiotis VA. Selective effects of PD-1 on Akt and Ras pathways regulate molecular components of the cell cycle and inhibit T cell proliferation. *Science Signaling* (2012) 5(230):ra46.

Peggs KS, Quezada SA, Allison JP. Cancer immunotherapy: co-stimulatory agonists and co-inhibitory antagonists. *Clinical and Experimental Immunology* (2009) 157(1):9–19.

Pennock GK, Chow LQ2. The Evolving Role of Immune Checkpoint Inhibitors in Cancer Treatment. *Oncologist* (2015) 20(7):812-22.

Pepper LR, Cho YK, Boder ET, Shusta EV. A decade of yeast surface display technology: where are we now? *Combinatorial Chemistry and High Throughput Screening* (2008) 11(2):127-34.

Postow MA, Chesney J, Pavlick AC, Robert C, Grossmann K, McDermott D, Linette GP, Meyer N, Giguere JK, Agarwala SS, Shaheen M, Ernstoff MS, Minor D, Salama AK, Taylor M, Ott PA, Rollin LM, Horak C, Gagnier P, Wolchok JD, Hodi FS. Nivolumab and ipilimumab versus ipilimumab in untreated melanoma. *New England Journal of Medicine* (2015) 372(21):2006–17.

Rajpal A, Beyaz N, Haber L, Cappuccilli G, Yee H, Bhatt RR, Takeuchi T, Lerner RA, Crea R. A general method for greatly improving the affinity of antibodies by using combinatorial libraries. *Proceedings of the National Academy of Sciences USA* (2005) 102(24):8466–8471.

Rao BM, Driver I, Lauffenburger DA, Wittrup KD. Interleukin 2 (IL-2) variants engineered for increased IL-2 receptor alpha-subunit affinity exhibit increased potency arising from a cell surface ligand reservoir effect. *Molecular Pharmacology* (2004) 66(4):864-9.

Rasila TS, Pajunen MI, Savilahti H. Critical evaluation of random mutagenesis by error-prone polymerase chain reaction protocols,

Escherichia coli mutator strain, and hydroxylamine treatment. *Analytical Biochemistry* (2009) 388(1):71–80.

Reck M, Heigener DF, Mok T, Soria JC, Rabe KF. Management of non-small-cell lung cancer: recent developments. *Lancet* (2013) 382(9893):709-19.

Reichert JM. Antibodies to watch in 2017. *Mabs* (2017) 9(2):167–181.

Riley JL. PD-1 signaling in primary T cells. *Immunological Reviews* (2009) 229(1): 114–125.

Robert C, Schachter J, Long GV, Arance A, Grob JJ, Mortier L, Daud A, Carlino MS, McNeil C, Lotem M, Larkin J, Lorigan P, Neyns B, Blank CU, Hamid O, Mateus C, Shapira-Frommer R, Kosh M, Zhou H, Ibrahim N, Ebbinghaus S, Ribas A. Pembrolizumab versus ipilimumab in advanced melanoma. *New England Journal of Medicine* (2015) 372(26):2521–32.

Roth DB. V(D)J Recombination: Mechanism, Errors, and Fidelity. *Microbiology Spectrum* (2014) 2(6).

Rozali EN, Hato SV, Robinson BW, Lake RA, Joost Lesterhuis W. Programmed Death Ligand 2 in Cancer-Induced Immune Suppression. *Clinical and Developmental Immunology* Volume 2012, Article ID 656340, 8 pages.

Rudnick SI, Adams GP. Affinity and Avidity in Antibody-Based Tumor Targeting. *Cancer Biotherapy and Radiopharmaceuticals* (2009) 24(2):155–161.

Sambrook J, Fritsch EF, Maniatis T. Molecular Cloning: A Laboratory Manual, Second Edition, Cold Spring Harbor Laboratory Press, Cold Spring Harbor, New York, 9.16 (1989).

Selenko-Gebauer N, Majdic O, Szekeres A, Höfler G, Guthann E, Korthäuer U, Zlabinger G, Steinberger P, Pickl WF, Stockinger H, Knapp W, Stöckl J. B7-H1 (programmed death-1 ligand) on dendritic cells is involved in the induction and maintenance of T cell anergy. *Journal of Immunology* (2003) 170(7):3637–44.

Seliger B, Cabrera T, Garrido F, Ferrone S. HLA class I antigen abnormalities and immune escape by malignant cells. *Seminars in Cancer Biology* (2002) 12(1):3–13.

Seliger B, Hohne A, Knuth A, Bernhard H, Ehring B, Tampe R, Huber C. Reduced membrane major histocompatibility complex class I density and stability in a subset of human renal cell carcinomas with low TAP and LMP expression. *Clinical Cancer Research* (1996) 2(8):1427–1433.

Sensi M, Anichini A. Unique tumor antigens: evidence for immune control of genome integrity and immunogenic targets for T cell-mediated patient-specific immunotherapy. *Clinical Cancer Research* (2006) 12(17):5023-32.

Sheppard KA, Fitz LJ, Lee JM, Benander C, George JA, Wooters J, Qiu Y, Jussif JM, Carter LL, Wood CR, Chaudhary D. PD-1 inhibits T-cell receptor induced phosphorylation of the ZAP70/CD3zeta signalosome and downstream signaling to PKC theta. *FEBS Letters* (2004) 574(1–3):37–41.

Siegel RW, Feldhaus M, Marks JD. Molecular evolution of antibody affinity for sensitive detection of botulinum neurotoxin type A. *Journal of Molecular Biology* (2005) 351(1):158–169.

Snyder A, Chan TA. Immunogenic peptide discovery in cancer genomes. *Current Opinion in Genetics & Development* (2015) 30:7-16.

Stavnezer J, Guikema JE, Schrader CE. Mechanism and regulation of class switch recombination. *Annual Reviews of Immunology* (2008) 26:261-92.

Sugita S, Usui Y, Horie S, Futagami Y, Aburatani H, Okazaki T, Honjo T, Takeuchi M, Mochizuki M. T-cell suppression by programmed cell death 1 ligand 1 on retinal pigment epithelium during inflammatory conditions. *Investigative Ophthalmology and Visual Science* (2009) 50(6):2862–70.

Sundberg EJ, Mariuzza RA. Molecular recognition in antibody-antigen complexes. *Advances in Protein Chemistry* (2002) 61:119–60.

Taube JM, Anders RA, Young GD, Xu H, Sharma R, McMiller TL, Chen S, Klein AP, Pardoll DM, Topalian SL, Chen L. Colocalization of inflammatory response with B7-h1 expression in human melanocytic lesions supports an adaptive resistance mechanism of immune escape. *Science Translational Medicine* (2012) 4(127):127ra37.

Tillotson BJ, Cho YK, Shusta EV. Cells and cell lysates: A direct approach for engineering antibodies against membrane proteins using yeast surface display. *Methods* (2013) 60(1):27-37.

Tillotson BJ, de Larrinoa IF, Skinner CA, Klavas DM, Shusta EV. Antibody affinity maturation using yeast display with detergent solubilized membrane proteins as antigen sources. *Protein Engineering, Design and Selection* (2013) 26(2):101–112.

Wang T, Niu G, Kortylewski M, Burdelya L, Shain K, Zhang S, Bhattacharya R, Gabrilovich D, Heller R, Coppola D, Dalton W, Jove R, Pardoll D, Yu H. Regulation of the innate and adaptive immune responses by Stat-3 signaling in tumor cells. *Nature Medicine* (2004) 10(1):48–54.

Wang XX, Cho YK, Shusta EV. Mining a yeast library for brain endothelial cell-binding antibodies. *Nature Methods* (2007) 4(2):143-5.

Wang XX, Shusta EV. The use of scFv-displaying yeast in mammalian cell surface selections. *Journal of Immunological Methods* (2005) 304(1-2):30–42.

Weber JS, D'Angelo SP, Minor D, Hodi FS, Gutzmer R, Neyns B, Hoeller C, Khushalani NI, Miller WH Jr, Lao CD, Linette GP, Thomas L, Lorigan P, Grossmann KF, Hassel JC, Maio M, Sznol M, Ascierto PA, Mohr P, Chmielowski B, Bryce A, Svane IM, Grob JJ, Krackhardt AM, Horak C, Lambert A, Yang AS, Larkin J. Nivolumab versus chemotherapy in patients with advanced melanoma who progressed after anti-CTLA-4 treatment (CheckMate 037): a randomised, controlled, open-label, phase 3 trial. *Lancet Oncology* (2015) 16(4):375–84.

Wolchok JD, Hodi FS, Weber JS, Allison JP, Urba WJ, Robert C, O'Day SJ, Hoos A, Humphrey R, Berman DM, Lonberg N, Korman AJ. Development of ipilimumab: A novel immunotherapeutic approach for the treatment of advanced melanoma. *Annals of the New York Academy of Sciences* (2013) 1291:1–13.

Yoshinaga K, Matsumoto M, Torikai M, Sugyo K, Kuroki S, Nogami K, Matsumoto R, Hashiguchi S, Ito Y, Nakashima T, Sugimura K. Ig L-chain shuffling for affinity maturation of phage library-derived human anti-human MCP-1 antibody blocking its chemotactic activity. *Journal of Biochemistry* (2008) 143(5):593-601.

Zhang X, Schwartz JC, Guo X, Bhatia S, Cao E, Lorenz M, Cammer M, Chen L, Zhang ZY, Edidin MA, Nathenson SG, Almo SC. Structural and functional analysis of the costimulatory receptor programmed death-1. *Immunity* (2004) 20(3):337–47.

Zhong X, Tumang JR, Gao W, Bai C, Rothstein TL. PD-L2 expression extends beyond dendritic cells/macrophages to B1 cells enriched for V(H)11/V(H)12 and phosphatidylcholine binding. *European Journal of Immunology* (2007) 37(9):2405–10.